UNCLASSIFIED

The Smoke Hazards Resulting From the Burning of Shipboard Materials Used by the U.S. Navy

B. T. ZINN, R. F. BROWNER, E. A. POWELL, M. PASTERNAK, AND R. O. GARDNER

Georgia Institute of Technology
School of Aerospace Engineering
Atlanta, Georgia

July 22, 1980

This report was prepared by Georgia Institute of Technology, School of Aerospace Engineering, under Contract N00014-78-6-0771 for the Combustion and Fuels Branch, Naval Research Laboratory

NAVAL RESEARCH LABORATORY
Washington, D.C.

Approved for public release; distribution unlimited.

REPORT DOCUMENTATION PAGE

READ INSTRUCTIONS BEFORE COMPLETING FORM

1. REPORT NUMBER: NRL Report 8414
2. GOVT ACCESSION NO.:
3. RECIPIENT'S CATALOG NUMBER:

4. TITLE (and Subtitle): THE SMOKE HAZARDS RESULTING FROM THE BURNING OF SHIPBOARD MATERIALS USED BY THE U.S. NAVY

5. TYPE OF REPORT & PERIOD COVERED: 1 Sept. 1978 - 31 Aug. 1979

6. PERFORMING ORG. REPORT NUMBER:

7. AUTHOR(s): B. T. Zinn, R. F. Browner, E. A. Powell, M. Pasternak, and R. O. Gardner

8. CONTRACT OR GRANT NUMBER(s): N00014-78-C-0771

9. PERFORMING ORGANIZATION NAME AND ADDRESS: Georgia Institute of Technology, School of Aerospace Engineering, Atlanta, Georgia 30332

10. PROGRAM ELEMENT, PROJECT, TASK AREA & WORK UNIT NUMBERS: 63514N; S0364-SL; 61-0061-0-0

11. CONTROLLING OFFICE NAME AND ADDRESS: Naval Research Laboratory, Washington, DC 20375

12. REPORT DATE: July 22, 1980

13. NUMBER OF PAGES: 63

14. MONITORING AGENCY NAME & ADDRESS (if different from Controlling Office):

15. SECURITY CLASS. (of this report): UNCLASSIFIED

15a. DECLASSIFICATION/DOWNGRADING SCHEDULE:

16. DISTRIBUTION STATEMENT (of this Report)

Approved for public release; distribution unlimited

17. DISTRIBUTION STATEMENT (of the abstract entered in Block 20, if different from Report)

18. SUPPLEMENTARY NOTES

Contract monitored by Frederick W. Williams
Code 6180
Naval Research Laboratory

19. KEY WORDS (Continue on reverse side if necessary and identify by block number)

Smoke
Combustion products
Particle size analysis
Light scattering
Polymeric materials
Chemical analysis
Toxic compounds
Fire hazards

20. ABSTRACT (Continue on reverse side if necessary and identify by block number)

A study has been conducted to evaluate the hazards due to smoke formation in shipboard fires. The physical and chemical properties of the smoke particulates generated during combustion were determined for representatives of the following three classes of materials abundantly present on shipboard: a wall insulation material, cable jacket materials, and a hydraulic fluid. Physical properties measured were particle size distribution and mean particle diameter, mass fraction of fuel converted to particulates, optical density, particle refractive index, and particulate volume fraction. The dependence of these properties on the temperature of the test-chamber atmosphere and the mode of combustion

(Continues)

UNCLASSIFIED

20. Abstract (Continued)

(flaming or smoldering) was determined. Chemical analysis of the smoke particulates determined the major toxic species generated during the combustion of these materials.

Results of this study indicate that these materials produce smoke particles with log-normal size distributions and mean diameters ranging from 0.4 to 1.5 μm (smoldering) and 1.0 to 1.3 μm (flaming). For these materials total particulate mass is greatest under smoldering combustion, and optical density is greatest under flaming combustion. For smoldering combustion, increasing ambient temperature reduces the mean diameter, peak optical density, volume fraction, and total particulate volume; ambient temperature has little effect upon these properties for flaming combustion. Toxic species identified during smoldering combustion include carbon monoxide, benzene, carbonyl sulfide, hydrogen chloride, acrolein and methacrolein.

UNCLASSIFIED

CONTENTS

PREFACE

This report was prepared by Georgia Institute of Technology, School of Aerospace Engineering, under contract N00014-78-6-0771 for the Combustion and Fuels Branch, Naval Research Laboratory.

This work was conducted to gain background information on the types of hazards one could expect from the burning of typical materials found in the confines of Navy ships. Three of the more prevalent materials often involved in fires (hull insulation, cable jacketing and hydraulic fluid) were evaluated under both flaming and nonflaming heat stresses. The "smoke" produced from these materials was both physically and chemically characterized. The smoke as defined here involves the gaseous, and gas adsorbed on particulate products.

This report has been reviewed by Drs. Frederick W. Williams and Homer W. Carhart of the Combustion and Fuels Branch, Naval Research Laboratory.

UNCLASSIFIED

THE SMOKE HAZARDS RESULTING FROM THE BURNING OF SHIPBOARD MATERIALS USED BY THE U.S. NAVY

INTRODUCTION

This report describes work for the Naval Research Laboratory between September 1, 1978, and August 31, 1979, concerned with the evaluation of the hazards due to smoke formation in shipboard fires. Specifically, the major objective of this 1-year research program was the determination of the physical and chemical properties of smoke particulates generated during the combustion of representatives of three classes of materials abundantly present on shipboard. The aims of this investigation were: the identification of conditions under which large quantities of smoke that would cause severe light obscuration are generated, the identification of major toxic species which are associated with the smoke particulates generated during the combustion of the above-mentioned materials, and the identification of compounds present in the smoke particulates which are possible precursors to smoke formation.

The efforts of this research project were divided into two major tasks. Task A is concerned with the measurements of the physical properties of the smoke particulates, and task B deals with the chemical analysis of the combustion products. Task B was subdivided into two subtasks: chemical analysis of major toxic volatile species in the smoke from tested samples and chemical analysis of possible precursors to smoke formation.

This program was directed by Dr. Ben. T. Zinn in the School of Aerospace Engineering of the Georgia Institute of Technology. He was assisted by Dr. R. F. Browner in the School of Chemistry, who was responsible for the chemical analysis work under task B. Other senior staff members participating in the research were Drs. E. A. Powell and M. Pasternak and Mr. B. R. Daniel.

EXPERIMENTAL FACILITIES

The smoke research program described herein used the following facilities which have been developed at the School of Aerospace Engineering, Georgia Institute of Technology: a combustion products test chamber, a combustion products sampling system, an in situ optical aerosol measurement system, and a chemical analysis laboratory.

The ventilated combustion products test chamber (CPTC) shown in Fig. 1 can simulate a wide variety of environmental conditions that may be encountered in actual fire situations. Specifically, the design of the CPTC permits easy control and measurement of the following variables during the combustion of small samples of materials: the mode of combustion (flaming vs smoldering combustion), the sample radiant heating rate (up to

Manuscript submitted April 7, 1980.

10 W/cm^2), the sample weight loss during the test, the composition of the ventilating gas surrounding the sample, the temperature of the ventilation gas (up to 650°C), and an option to test the sample under either vertical or horizontal mounting. A complete description of the CPTC including operating procedures can be found in Refs. 1 and 2.

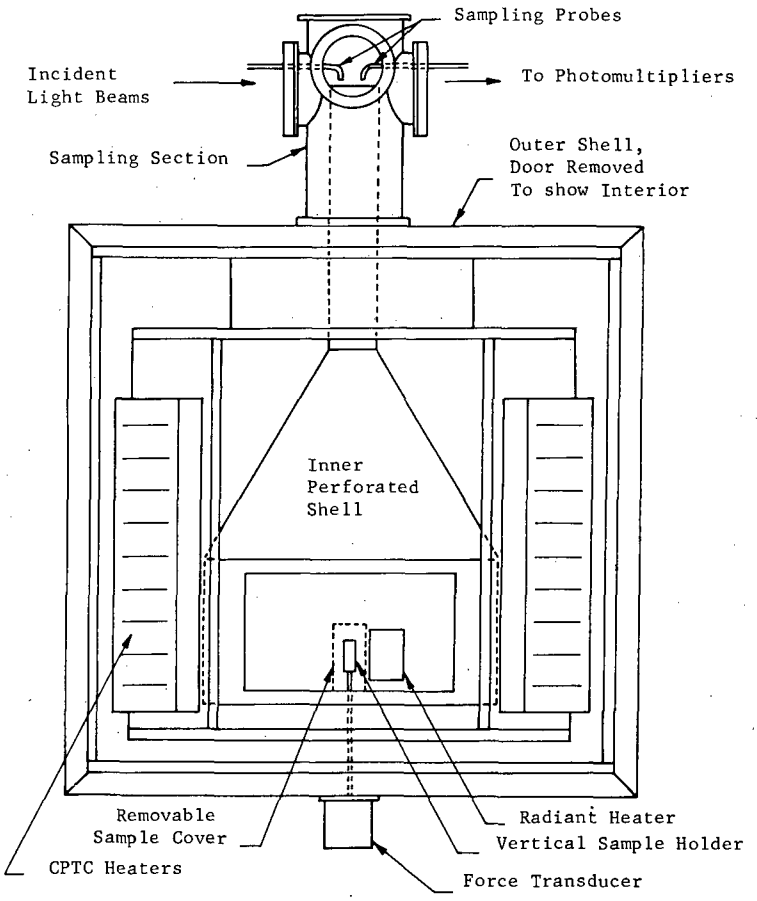

Fig. 1 — Combustion products test chamber

During testing, a combustion products sampling system (Fig. 2) is used to analyze smoke samples that are continuously withdrawn from the gases flowing from the CPTC. Information obtained by the aerosol sampling system includes particle size distributions and total particulate mass generated. Some of the collected smoke samples are also retained for chemical analysis. A description of the sampling system also can be found in Refs. 1 and 2.

In addition to the data obtained by sampling techniques, an in situ optical aerosol measurement system is used to make simultaneous mean particle size and concentration measurements (Fig. 3). With this optical smoke analysis system, measurement of scattered

UNCLASSIFIED

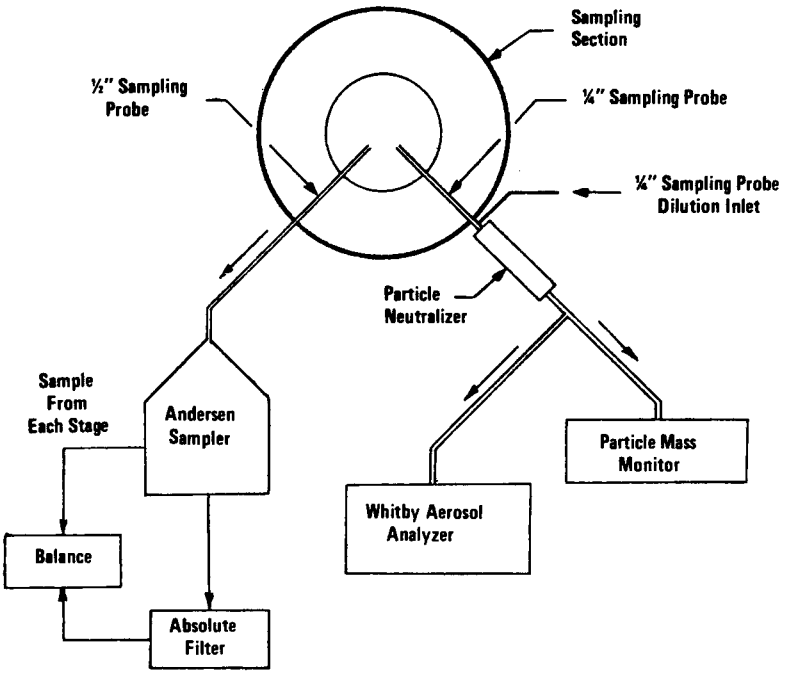

Fig. 2 — Combustion products sampling system

blue laser light (λ = 0.458 μm) at forward angles of 5° and 15° provide time-resolved data describing the average size of the smoke particles. Measurements of transmitted red (λ = 0.633 μm) and blue laser lights provide the optical densities of the smoke at these two wavelengths. For nonabsorbing particles (usually produced by nonflaming combustion) the transmitted light measurements along with the mean particle size measurements also yield the refractive index and volume concentration of the smoke particles. For absorbing particles (soot) measurements of 90°-scattered light intensities parallel to and perpendicular to the plane of polarization of the incident light beam (Fig. 4) provide additional data necessary to determine the complex refractive index of the smoke particles. Details of the optical system are available in Refs. 2, 3, and 4.

An on-line data acquisition system using a Hewlett-Packard 2100 minicomputer is used for acquiring, reducing, and plotting all of the optical and sampling data with the exception of Anderson Sampler (cascade impactor) data, which call for the weighing of the samples collected on the various impaction plates.

Finally, a chemical laboratory containing analytical equipment for the determination of the chemical composition of smoke particulates sampled during tests in the CPTC has been developed. The available equipment includes a high-pressure liquid chromatograph, an infrared spectrophotometer, a gas chromatograph equipped with a thermal conductivity detector, and a gas chromatograph which is equipped with dual flame ionization detectors and is interfaced to a mass spectrometer. The gas chromatograph/mass spectrometer system is also equipped with a computerized data acquisition and analysis system that records the

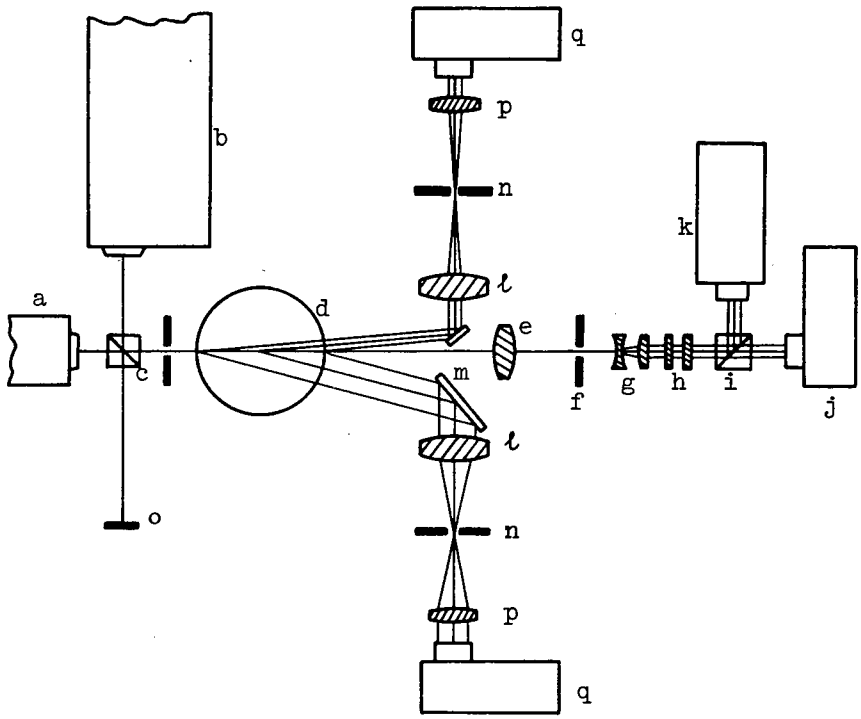

Fig. 3 — In situ optical aerosol measurement system:
(a) helium-neon laser,
(b) Argon-ion laser,
(c) beam-combining cube,
(d) 11.4-cm-diam stack from the combustion products test chamber,
(e) objective lens,
(f) pinhole aperture,
(g) beam expander,
(h) neutral density filters,
(i) beam-splitter cube,
(j) transmitted blue-light detector,
(k) transmitted red-light detector,
(l) objective lenses,
(m) mirrors,
(n) pinhole apertures,
(o) light stop,
(p) collimating lenses,
(q) 5°-scattering detector, and
(r) 15°-scattering detector

UNCLASSIFIED

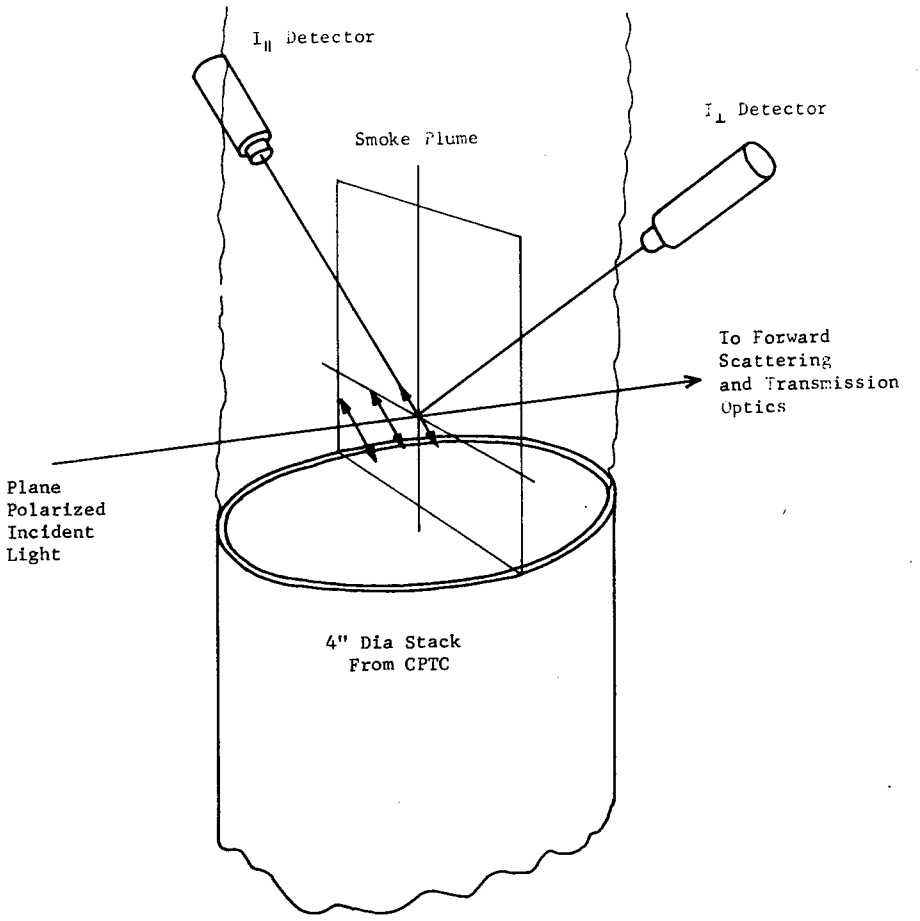

Fig. 4 — Optical system for 90°-scattering measurements

total-ion chromatograms and the mass spectra. A digital plotter is available for obtaining high-quality reproductions of the recorded data. Identification of the individual mass spectra is accomplished with the aid of the Aldermaston Spectral Library. Also, a recent addition to the chemical laboratory is a small combustion chamber and sampling system. This facility has been assembled for the accurate analysis of toxic gases absorbed on smoke particulates in conjunction with the above-described chemical analysis instrumentation.

PHYSICAL PROPERTIES OF THE SMOKE PARTICULATES PRODUCED BY BURNING SHIPBOARD MATERIALS

Task A of this research program was concerned with the determination of the detailed physical properties of smoke particulates generated by burning the following materials which have shipboard applications: a wall insulation material, a cable jacket material, and a hydraulic fluid. The materials and fluid to be tested were provided by the Navy. The tests

were performed by using the combustion products test chamber (CPTC), the aerosol sampling system, and the in situ aerosol measurement system.

For tests conducted in room-temperature ventilation gas, the physical analysis of the smoke particulates determined the following smoke properties: the particle size distribution, the mass fraction of fuel converted to particulates, the evolution of the mean particle diameter with time, the light obscuration by the particles (optical density), the particle refractive index, and the volume fraction (volume concentration) of the particles. For the tests conducted in hot ventilation gas, the particle size distribution and the mass fraction of fuel converted to particulates were not determined, since the aerosol sampling system cannot be operated at high temperature. In addition, the sample mass loss as a function of time was determined for most of the tests.

The dependence of the above quantities on the following experimental conditions was determined: the temperature of the test chamber atmosphere, and the mode of combustion (flaming or smoldering combustion). Thus the three materials were subjected to the test matrix shown in Table 1. All of the materials were tested in the horizontal orientation and were exposed to a radiant heat flux of 5 W/cm^2. In the flaming tests, the pyrolysis products generated by exposure of the sample to the 5-W/cm^2 radiant flux were ignited by a small propane pilot flame. For some of the test conditions imposed, nonflaming data were unobtainable due to spontaneous ignition of the pyrolysis products (due to radiative and convective heating alone without the aid of a pilot flame). Spontaneous ignition of the hydraulic fluid occurred at all temperatures tested, and all three materials ignited in the 300°C atmosphere. Thus the maximum ventilation gas temperature used in the nonflaming tests was 200°C. Finally, in all tests the CPTC ventilation gas consisted of air flowing at a volumetric rate (before heating) of 425 liters per minute. Due to the decrease in density of the ventilation air during heating, the volumetric flow rate of the heated air during the high-temperature tests was higher, as shown in Table 1.

Table 1 — Test Program

Test	Ventilation Gas Temperature (°C)	Type of Combustion	Radiant Flux (W/cm^2)	Ventilation Gas Composition	Flow Rate of Heated Ventilation Gas (l/min)
1	25	Nonflaming	5.0	Air	425
2	100	Nonflaming	5.0	Air	532
3	200	Nonflaming	5.0	Air	675
4	25	Flaming	5.0	Air	425
5	100	Flaming	5.0	Air	532
6	300	Flaming	5.0	Air	817

In the following sections of this report smoke particulate physical properties data will be presented for each of the three materials tested during this research program. Before presenting these data, a brief discussion of each of the measured parameters is given in the following subsections.

UNCLASSIFIED

Particle Size Distribution

Particle size distributions are presented as cumulative curves which are generated by plotting the percentage of particulate weight having particle diameters less than a given particle size versus the particle size on log-normal probability paper [5]. These data are taken from Andersen Sampler (cascade impactor) measurements, and when the weight distribution of the particle sizes is log-normally distributed, the curves appear as straight lines [5]. Also, when the mass-size distribution is log-normally distributed, the number and surface-size distributions are also log-normally distributed with the same standard deviation [5]. In the presentation of these data, the cumulative size distribution plots have been represented when practicable by a straight line corresponding to a log-normal distribution. When the data could not reasonably be represented by a straight line, two straight lines were fitted to the data points instead. The mass median diameter (D_{MMD}) is readily obtained from these cumulative probability plots; 50% of the sampled particulates (by mass) are composed of particles of diameters less (or greater) than the mass median diameter [5]. The geometric standard deviation (σ_g) is also calculated from the log-normal plots according to the following formula given by Cadle [5]:

$$\sigma_g = \frac{D(84.13\%)}{D_{MMD}} = \frac{D_{MMD}}{D(15.87\%)} .$$

The geometric standard deviation is an indication of the relative spread of particle diameters about the mean diameter such that about 68% of the particles have diameters between D_{MMD}/σ_g and $\sigma_g D_{MMD}$. Although the data shown do not always follow a log-normal distribution, the authors believe that the values of σ_g calculated from the cumulative probability plots gives a general indication of the dispersity of the data, thus providing a reasonable basis for comparisons.

Mass Fraction of Fuel Converted to Particulates

The weight of the collected particulates is used to calculate the fraction of the sample weight loss which becomes particulate matter (Γ). This provides an indication of the tendency of a material to generate smoke per unit mass of fuel expended.

Mean Particle Diameter

The forward-scattering light-intensity measurements obtained with the in situ optical aerosol measurements system were used to determine the volume-surface mean particle diameter (D_{32}) as a function of time during each test. The volume-surface mean diameter is defined as follows:

$$D_{32} = \frac{\int_0^{D_\infty} N(D) D^3 \, dD}{\int_0^{D_\infty} N(D) D^2 \, dD} ,$$

where $N(D)$ is the number size distribution, D is the particle diameter, and D_∞ is the maximum particle diameter. Using blue light from an argon-ion laser (λ = 458 nm), measurements were made of the ratio of scattered light intensities at two forward angles (5° and 15°), from which D_{32} was determined by diffractive scattering theory [6]. The measurement of D_{32} by this forward scattering ratio technique is relatively insensitive to the particle refractive index and concentration (unknown) and the shape of the size distribution function. In calculating D_{32} from the measured intensity ratio, the "upper limit distribution function" used by Mugele and Evans [7] and later by Dobbins and Jizmagian [8] was assumed. In addition to the plots of D_{32} versus time, the value of D_{32} corresponding to maximum light obscuration (peak optical density) was determined for each test.

Optical Density

The transmitted blue light from the argon-ion laser and the transmitted red light from a He-Ne laser (λ = 633 nm) were used to determine the optical densities at these two wavelengths as a function of time. The smoke optical density per unit optical path length is defined as follows:

$$OD = \frac{\log_{10} \frac{I_0}{I}}{L},$$

where I_0 is the incident light intensity, I is the light intensity transmitted through the smoke, and L is the optical path length (0.114 m for the CPTC). These data are presented as plots of the optical density in blue light (OD_B) versus time. In addition maximum optical densities (OD_{max}) at both wavelengths were determined for each test. The increased dilution of the smoke by the higher volumetric flow rate of the hot ventilation air in the high-temperature tests (Table 1) tends to reduce the optical density of the smoke. To eliminate this dilution effect, the high-temperature OD_{max} data has been corrected to the same volumetric flow rate as the 25°C data using the formula

$$OD_{corr} = OD_{meas} \left(\frac{\dot{V}_t}{\dot{V}_{25}} \right) = OD_{meas} \left(\frac{T + 273}{298} \right),$$

where $\dot{V}_T$ and $\dot{V}_{25}$ are the volumetric flow rates at high temperature and at 25°C respectively and T is the ventilation gas temperature in degrees Celsius.

Particle Refractive Index

To obtain the volume concentration of the smoke particles from the measured optical densities and mean particle diameters, it is necessary to know the refractive index ($m = n - ik$) of the smoke particles. It has been shown in Ref. 3 for nonabsorbing spherical particles of known D_{32} that the real part of the refractive index n (the imaginary part is zero) can be determined from the ratio of optical densities at two widely separated

UNCLASSIFIED

wavelengths, provided the refractive index is independent of wavelength. Thus measurements of the ratio of optical density in red light (λ = 633 nm) to the optical density in blue light (λ = 458 nm) were made for each of the materials studied in task A. This optical density ratio (OD_R/OD_B) along with the measured values of D_{32} was used to calculate values of n for the nonflaming tests, since smoke particulates produced under nonflaming conditions usually consist of tarry liquid droplets which are assumed to be nonabsorbing; that is, the imaginary part (absorption index k) of the refractive index is either zero or very small.

The above method of determining the refractive index of smoke particles fails if the smoke particles have significant values of the absorption index k. To determine both n and k, additional information is needed. Thus two additional detectors have been incorporated into the optical system to measure red light (λ = 633 nm) scattered in the plane perpendicular to the incident light beam. These detectors measure the 90°-scattering intensities parallel to ($I_\parallel$) and perpendicular to ($I_\perp$) the plane of polarization of the incident light beam. Using the Mie scattering theory [9], the ratio of $I_\parallel/I_\perp$ can be used along with the mean particle size D_{32} (from the forward scattering measurements) and the ratio of optical densities at the two laser wavelengths to obtain the complex refractive index m of the smoke particles. In practice the values of n and k can be determined from measurements of D_{32}, OD_R/OD_B, and $I_\parallel/I_\perp$ only if the absorption index k is not too large ($k < 0.4$), n and k are both independent of wavelength for the wavelengths used, and the smoke particles are spherical and homogeneous.

Values of $I_\parallel/I_\perp$ were measured for most of the tests conducted under Task A. For the *nonflaming* tests the measured values of $I_\parallel/I_\perp$ and D_{32} were used to calculate the refractive index n under the assumption of k = 0. Comparison of these values of n with the values of n calculated from the OD_R/OD_B measurements were used to check the validity of the assumptions of k = 0 and of wavelength independence of n for the smoke produced in smoldering combustion. For *flaming* combustion the particulates consist of highly absorbing carbonaceous material (soot) with a refractive index of approximately $m = 1.57 - 0.56i$ [10]. Thus the values of $I_\parallel/I_\perp$ and OD_R/OD_B measured in the flaming tests are compared with the values computed using the Mie theory with $m = 1.57 - 0.56i$.

Particulate Volume Fraction

The concentration of the smoke particles is determined from the optical density in terms of the particulate volume fraction or volume concentration, which is the volume of particles contained in a unit volume of gas-particle mixture (aerosol). With use of the previously determined mean particle diameters (D_{32}) and refractive index (m), the volume fraction (ϕ) was calculated from the red-light transmission measurements using the expression [3,8]

$$\phi = \frac{2}{3}\left[\frac{D_{32}}{\bar{Q}_{ext}(D_{32}, m)\, L}\right] \ln (I_0/I)_R,$$

where $\overline{Q}_{ext}$ is the mean extinction efficiency given [8] by

$$\overline{Q}_{ext} = \frac{\int_0^{D_\infty} Q_{ext}(D, m) N(D)\, D^2\, dD}{\int_0^{D_\infty} N(D) D^2\, dD}.$$

Thus plots of volume fraction ϕ versus time were obtained for each of the tests conducted in task A. In these plots the volume fractions for the high-temperature tests have been corrected to the standard flow rate of 425 l/min according to the formula

$$\phi_{corr} = \phi_{meas} \frac{\dot{V}_T}{\dot{V}_{25}} = \phi_{meas} \left(\frac{T + 273}{298} \right).$$

The total volume of smoke particulates produced during each test was then estimated by integrating the ϕ-versus-time curve and multiplying by the constant volumetric flow rate for the test:

$$V_p = \dot{V}_T \int_0^{t_{max}} \phi\, dt.$$

If the density of the particulates (ρ_p) is known, the total particulate mass is then given by

$$m_p = \rho_p\, V_p,$$

and the fraction of sample weight loss converted to particulates (Γ) is given by

$$\Gamma = \frac{m_p}{M_i - M_f},$$

where M_i and M_f are the initial and final sample masses respectively. Values of Γ thus obtained optically were then compared with the Γ values obtained from the collected samples for the low-temperature tests.

Sample Weight Loss

For each test the weight of the burning sample was monitored continuously, and the results are plotted as curves of percent initial weight versus time. From the maximum slope of the weight-loss curve the peak mass loss rate per unit sample area was also obtained. Finally the amount of char residue, if any, was determined as a percentage of the initial sample weight.

UNCLASSIFIED

SMOKE PHYSICAL PROPERTIES DATA FOR WALL INSULATION MATERIAL

The shipboard wall insulation material tested under task A was a black, flexible, polymeric foam material with a density of about 0.1 g/cm^3. This material was received from the Navy in the form of 30-cm squares about 2.5 cm thick. The bulk of this material was cellular, but the cell size decreased sharply within 2 mm of the upper and lower surfaces such that these surfaces were relatively smooth and nonporous. One surface (which will be designated as the upper surface) was much smoother and less porous than the other. In preparing the samples for testing, the material was cut into 7.6-cm squares with a thickness 1/2 that of the uncut material (about 12 mm). Only the half with the smoothest surface (the upper half) was tested, and the sample was always mounted horizontally with the smooth surface exposed to the radiant heat source. Sample weights ranged from 6.8 to 7.6 g.

Tests in Room-Temperature Ventilation Air

Both flaming and nonflaming tests of the wall insulation material were conducted under a radiant exposure of 5 W/cm^2 in room-temperature ventilation air (25°C) at a flow rate of 425 l/min. The results of these tests are presented in Figs. 5 through 8, in which flaming and nonflaming data are compared. These results are also included in Tables 2 and 3.

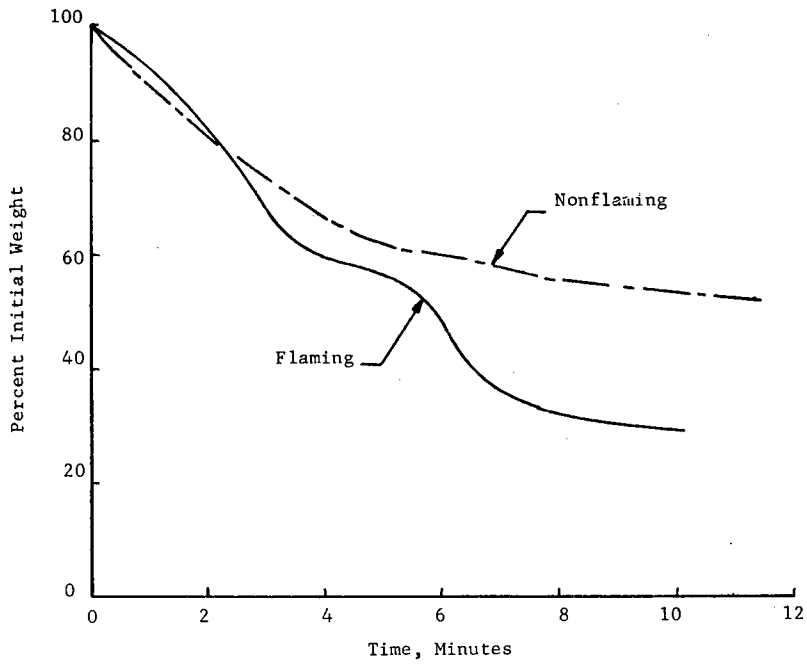

Fig. 5 — Sample weight losses for flaming and nonflaming combustion of wall insulation material exposed to a radiant flux of 5 W/cm^2 in room-temperature ventilation air (25°C)

Table 2 — Sample Weight Loss Data for Wall Insulation Material

Mode	Ventilation Air Temperature (°C)	Peak Mass Loss Rate (mg/cm^2-s)	Char Residue (% of Initial Weight)
Nonflaming	25	0.24	52
Nonflaming	100	0.26	54
Nonflaming	200	0.27	48
Flaming	25	0.34	34
Flaming	100	Not available	28
Flaming	300	1.09	23

Table 3 — Smoke Properties Data for Wall Insulation Material

Mode	Ventilation Gas Temperature (°C)	Γ	D_{MMD} (μm)	σ_g	OD_{max}		D_{32}* (μm)	Time to Peak OD (min)
					Blue	Red		
Nonflaming	25	0.059	0.65	1.67	1.94	1.48	0.62	1.02
Nonflaming	100	—	—	—	0.88	0.56	0.51	0.60
Nonflaming	200	—	—	—	0.29	0.11	0.44	0.85
Flaming	25	0.024	0.36	2.31	1.87	1.45	1.03	0.52
Flaming	100	—	—	—	1.84	1.46	1.08	0.53
Flaming	300	—	—	—	3.03	2.28	1.17	0.38

*Average for data points near the time of maximum optical density.

Curves of sample weight loss for flaming and nonflaming combustion of the wall insulation material are shown in Fig. 5. Peak mass loss rates and amounts of char residue obtained from these curves are given in Table 2. As expected, the sample mass loss rates are higher for flaming combustion due to the additional radiant heat flux to the sample surface contributed by the flame. In addition there was less char residue remaining after the test when flaming combustion occurred, which is also consistent with the higher radiant heat flux and resulting increased amount of pyrolysis products generated. During these tests, the originally flat samples bowed up into a dome shape, and visible smoke issued mainly from cracks which formed in the smooth upper surface. The char that remained after these tests appeared to be a black, brittle, carbonaceous material which retained the same cellular structure as the original polymer.

Smoke particle size distributions for flaming and nonflaming combustion are presented in Fig. 6. In both cases a straight line gives a good fit to the data (obtained from the cascade impactor), which indicates that the size distribution is log-normal. Mass median

UNCLASSIFIED

diameters (D_{MMD}) and standard deviations (σ_g) obtained from these curves are given in Table 3. These data indicate that the particulates produced during flaming combustion of this material have a considerably smaller mass median diameter and larger standard deviation (dispersion) than those produced under nonflaming conditions. Inspection of the collected samples showed that the particulates produced under nonflaming combustion consisted of a yellowish tarry liquid, whereas the particulates produced by flaming combustion were a mixture of black, carbonaceous material (soot) and a grayish material of unknown composition. The grayish material collected in the flaming tests was predominantly on the lower stages of the cascade impactor (0.43 to 1.1 μm) and on the absolute filter (< 0.43 μm). Sampling data were also used to determine the fraction of the sample mass loss converted to particulates Γ. These values of Γ are also given in Table 3, which show that larger values of Γ are obtained under nonflaming conditions.

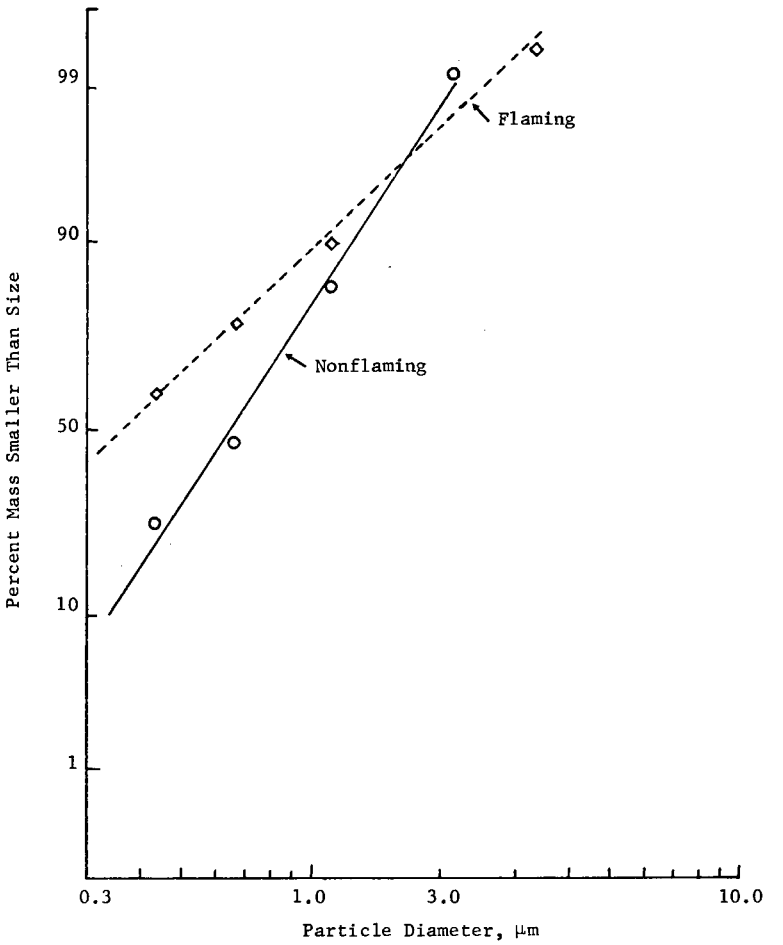

Fig. 6 — Smoke particle size distributions flaming and nonflaming combustion of wall insulation material exposed to a radiant flux of 5 W/cm^2 in room-temperature ventilation air (25°C)

Figure 7 shows the variation of the mean particle size (D_{32}) with time during flaming and nonflaming tests of the wall insulation material. For nonflaming combustion D_{32} gradually decreases as the test proceeds, ranging from about 0.7 μm shortly after initial exposure to about 0.3 μm after 8 minutes. Most of this decrease in D_{32} occurs during a period of declining mass loss rate, which is consistent with a reduction in the amount of condensible pyrolysis products available for particulate growth. For flaming combustion D_{32} is considerably larger (about 1.0 μm) during the first 2 minutes after ignition; thereafter D_{32} follows the same trends observed for nonflaming combustion. This indicates that the concentration of combustible pyrolysis products leaving the sample surface is insufficient to maintain flaming combustion after about 3 minutes.

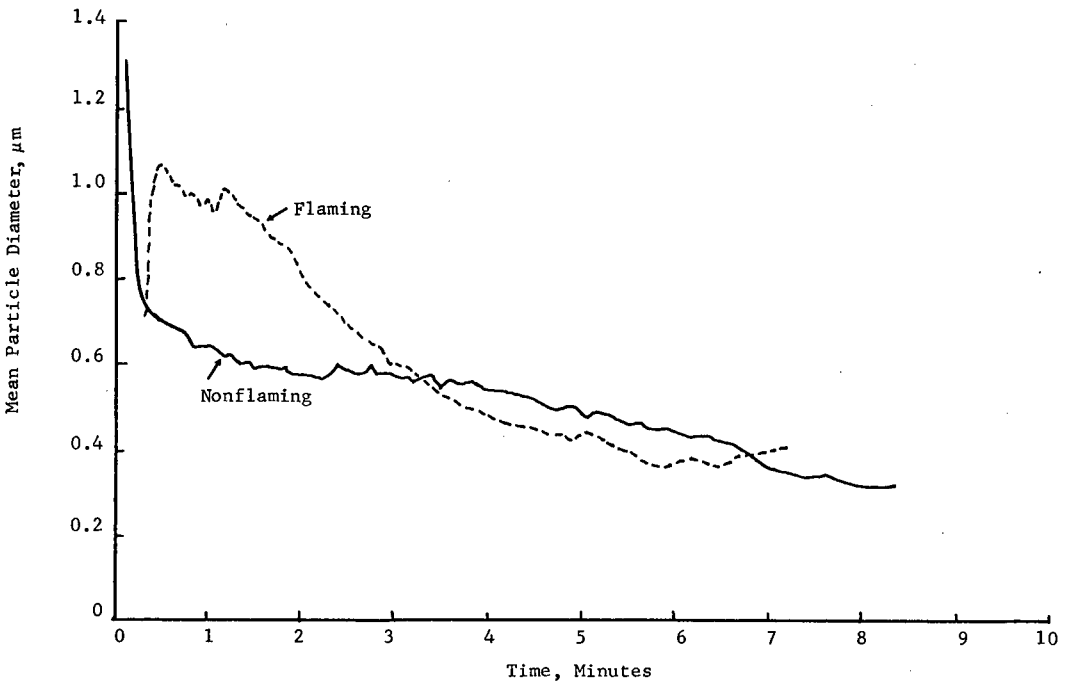

Fig. 7 — Smoke mean particle diameters for flaming and nonflaming combustion of wall insulation material exposed to a radiant flux of 5 W/cm^2 in room-temperature ventilation air (25°C)

Optical density (OD_B) variations during the same flaming and nonflaming tests are shown in Fig. 8. Peak optical density in red and blue light, time required to reach peak optical density, and the corresponding mean particle size at peak optical density are presented in Table 3. Although the peak optical densities for flaming and smoldering combustion of this material are nearly the same, the peak occurs earlier, is much sharper, and is followed by a more rapid decline in the case of flaming combustion.

Particle size data obtained with the in situ optical system can be readily compared with the corresponding sampling data by means of Table 3. For smoldering combustion the value of D_{MMD} obtained from the cascade impactor data and D_{32} at maximum light obscuration

UNCLASSIFIED

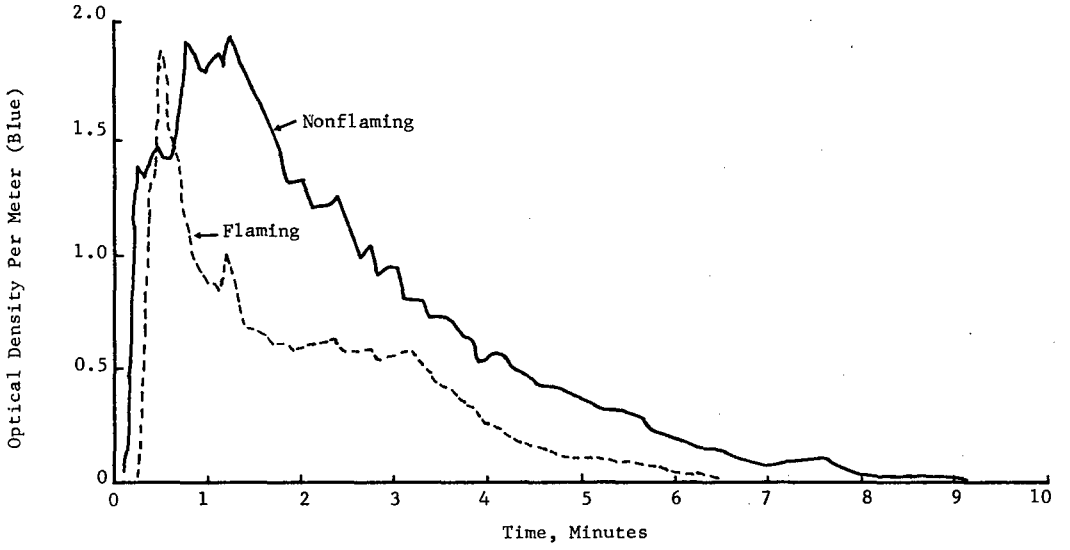

Fig. 8 — Smoke optical densities for flaming and nonflaming combustion of wall insulation material exposed to a radiant flux of 5 W/cm^2 in room-temperature ventilation air (25°C)

obtained from the light scattering measurements are in good agreement. In the case of flaming combustion, however, D_{MMD} is much smaller than the characteristic value of D_{32}. Such differences are expected, however, since the two mean diameters are defined differently, the D_{32} values are determined instantaneously but the D_{MMD} values are integrated averages for the entire test, and the sooty agglomerates produced in flaming combustion are generally nonspherical, leading to errors in both methods of measuring particle size.

Tests in Heated Ventilation Air

Results of tests of wall insulation material conducted in hot ventilation air are shown in Figs. 9 through 11 for nonflaming combustion and in Figs. 12 through 14 for flaming combustion. In each figure the room-temperature data are also shown for comparison. High-temperature data are also given in Tables 2 and 3. As given in Table 1, nonflaming tests were conducted at ventilation air temperatures of 100°C and 200°C, since flaming ignition occurred at 300°C. Flaming data were obtained at 100°C and 300°C.

Figure 9 and Table 2 show that ventilation air temperature has little effect on the curves of sample mass loss versus time, the peak mass loss rate, or the amount of char residue for *nonflaming* combustion of the wall insulation material. Thus exposure of this material to a radiant flux of 5 W/cm^2 at ambient temperature between 25°C and 200°C results in a maximum mass loss rate of about 0.25 mg/s per square centimeter of exposed surface area and a char residue of about 50% of the initial sample weight. At ambient temperatures above 300°C, radiant exposure to 5 W/cm^2 results in flaming ignition of the sample.

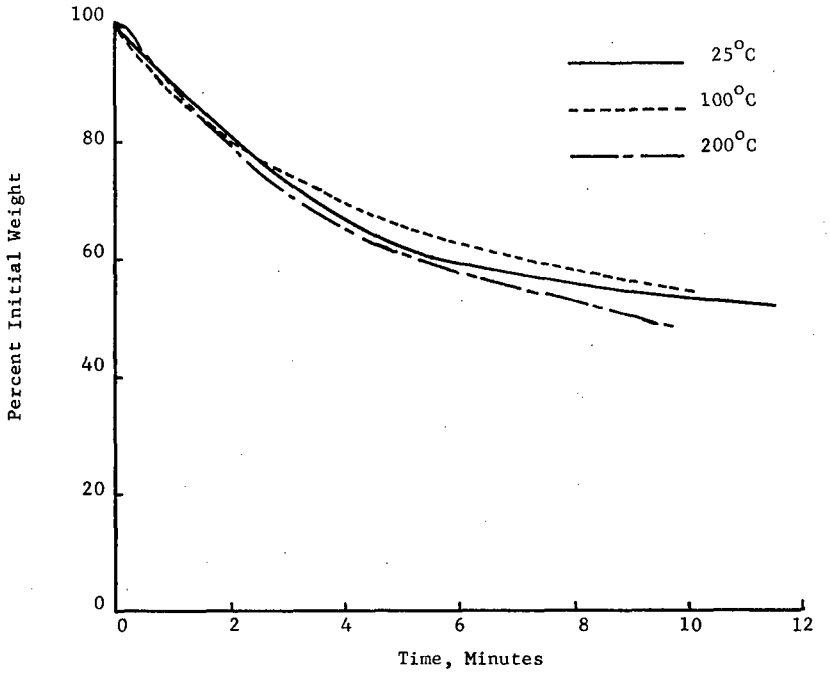

Fig. 9 — Effect of the ventilation air temperature on the sample weight loss for nonflaming combustion of wall insulation material exposed to a radiant flux of 5 W/cm^2

Mean particle diameters presented in Fig. 10 show that increasing the ventilation air temperature to 100°C and above reduces the size of the smoke particles produced in smoldering combustion of the wall insulation material. This trend of decreasing D_{32} with increasing environmental temperature is also shown by the data given in Table 3.

The optical density versus time curves shown in Fig. 11 and the peak optical density values given in Table 3 show a strong reduction in smoke optical density with increasing ambient temperature for nonflaming combustion of this material. When corrected for the increased dilution of the smoke at higher temperatures (Table 3), optical densities at 100°C and 200°C are respectively about 1/2 and 1/6 of the room-temperature values.

The above behavior of the mean particle diameter and the optical density as the environmental temperature is increased is readily explained if the formation and growth of smoke particles is controlled by the condensation of vapors produced by pyrolysis of the sample. Pyrolysis products with boiling points below the ambient temperature will not condense, and the condensation of materials with higher boiling points will be retarded as the temperature is increased. This reduces both the number of smoke particles produced as well as their rate of growth, resulting in a decrease in particle sizes and optical density.

The effect of ventilation air temperature on sample weight loss for *flaming* combustion of the wall insulation material is shown in Fig. 12. These curves and the data given in Table 2 show a threefold increase in the peak mass loss rate when the ambient temperature

UNCLASSIFIED

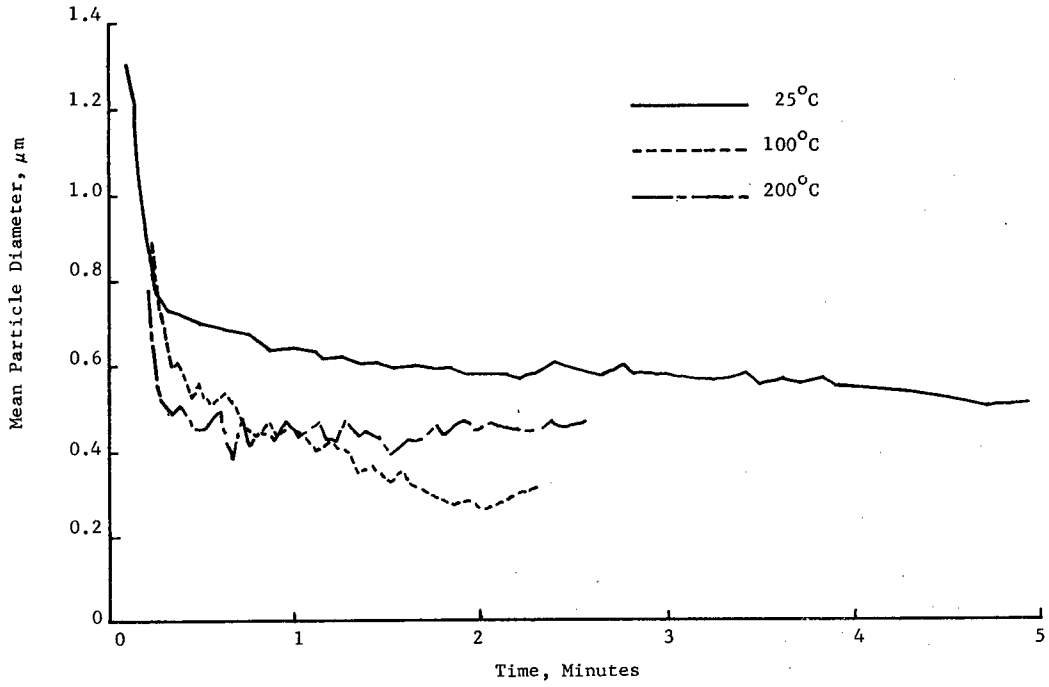

Fig. 10 — Effect of the ventilation air temperature on the smoke mean particle diameter for nonflaming combustion of wall insulation material exposed to a radiant flux of 5 W/cm^2

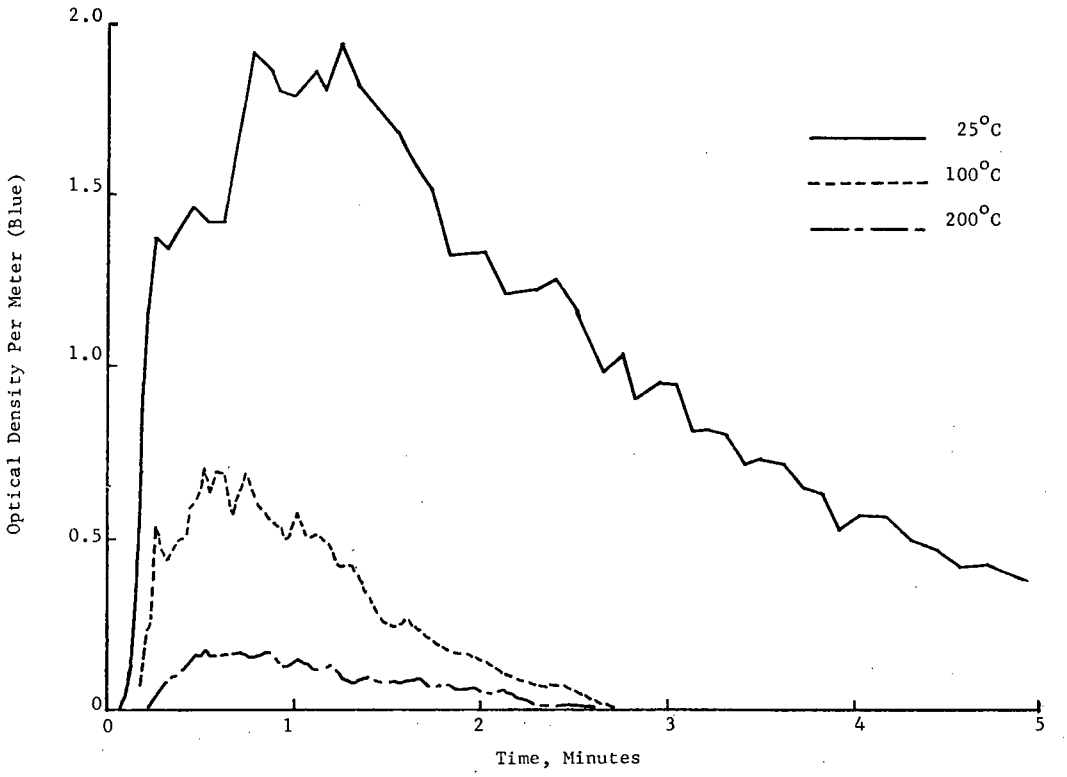

Fig. 11 — Effect of the ventilation air temperature on the smoke optical density for nonflaming combustion of wall insulation material exposed to a radiant flux of 5 W/cm^2

is raised form 25°C to 300°C. Also the amount of char residue decreases as the ventilation air temperature increases. At the highest temperature the char residue produced under flaming conditions consisted of a whitish ash, in contrast to the carbonaceous residue obtained under nonflaming conditions.

The curves of D_{32} versus time shown in Fig. 13 and the values of D_{32} at maximum optical density given in Table 3 indicate a small increase in mean particle size of the smoke produced by flaming combustion of the wall insulation material as the ambient temperature is increased from 25°C to 300°C. This behavior is opposite to that observed for nonflaming combustion, and it indicates that the condensation mechanism does not control the production and growth of the sooty smoke produced in flaming combustion. A different mechanism can be postulated to account for the behavior observed here. At higher ventilation air temperatures the rate of production of pyrolysis products (fuel) is increased (implied by the increased weight loss rates) while the mass flow rate of oxidizer (air) remains fixed. Thus combustion occurs under more fuel-rich conditions at high ambient temperature, which generally leads to greater quantities of soot particles produced in the flame. This enhances the agglomeration process in the smoke plume, which accounts for the larger particle sizes observed.

UNCLASSIFIED

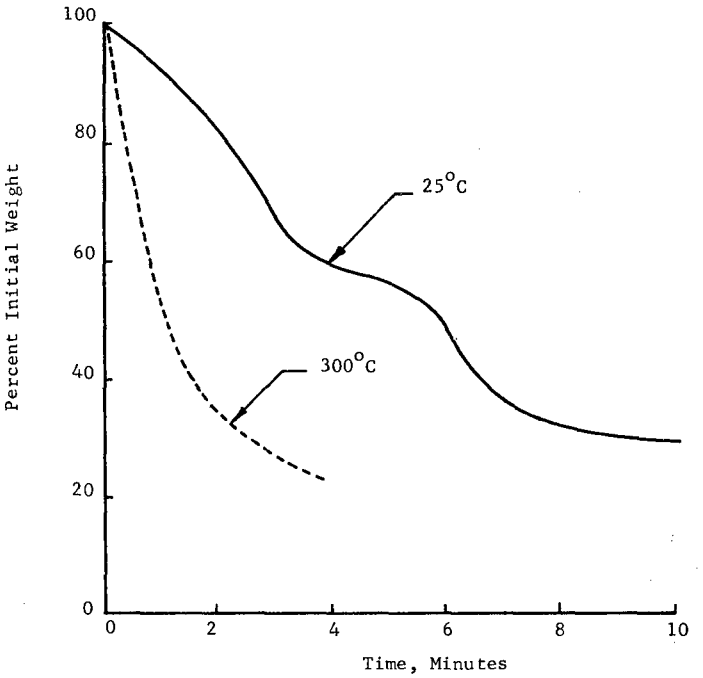

Fig. 12 — Effect of the ventilation air temperature on the sample weight loss for flaming combustion of wall insulation material exposed to a radiant flux of 5 W/cm^2

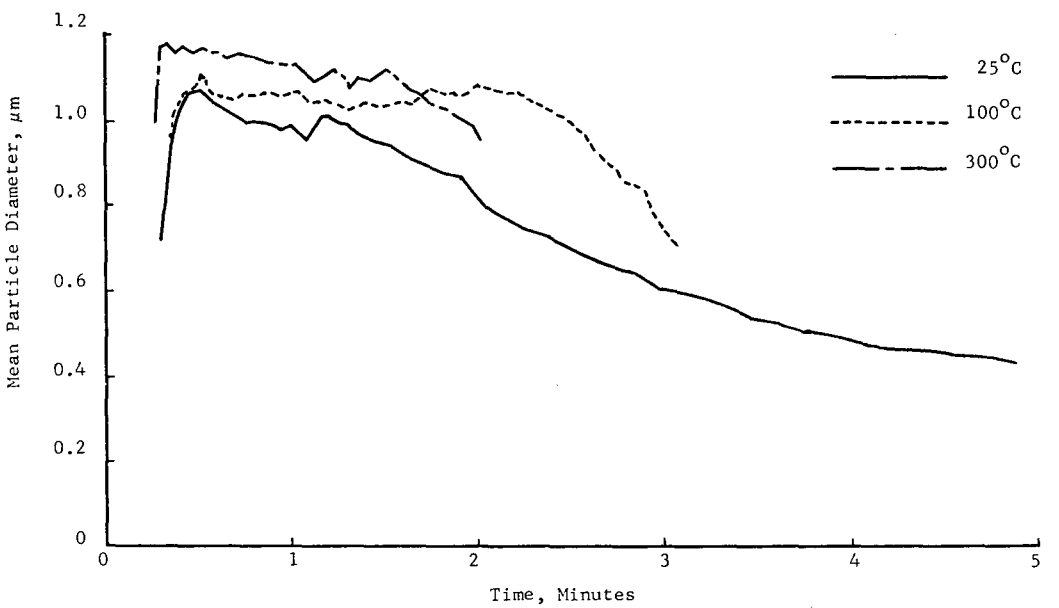

Fig. 13 — Effect of the ventilation air temperature on the smoke mean particle diameter for flaming combustion of wall insulation material exposed to a radiant flux of 5 W/cm^2

Optical density variations with time are presented in Fig. 14 for flaming tests of wall insulation material at elevated environmental temperatures. These curves, which are not corrected to the standard-room-temperature flow rate, show little effect of ambient temperature on the peak optical density obtained (1.5 to 2.0 m^{-1}). The corrected peak optical density values given in Table 3, however, show that the maximum optical density obtained at 300°C is nearly twice that obtained at room temperature or at 100°C. Also, significant light obscuration is produced over a shorter span of time at higher ambient temperatures. These results are consistent with the higher weight loss rates and increased amounts of soot produced under the fuel-rich conditions encountered at elevated environmental temperatures.

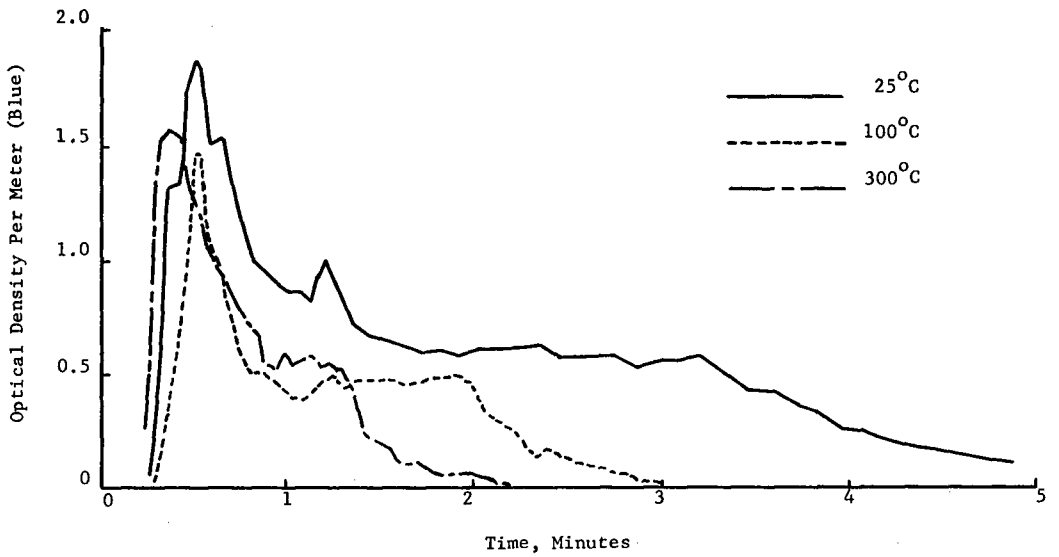

Fig. 14 -- Effect of the ventilation air temperature on the smoke optical density for flaming combustion of wall insulation material exposed to a radiant flux of 5 W/cm^2

Smoke Particle Refractive Index and Volume Fraction

For nonflaming tests of the wall insulation material, refractive indices (n) of the smoke particles were obtained with the assumption that the absorption index (k) was zero. Figure 15 shows the resulting variation of refractive index with time for the room-temperature test. Most of the values of n obtained from the optical density ratio (OD_R/OD_B) are in excellent agreement with the corresponding values of n obtained from the 90°-scattering ratio ($I_\parallel/I_\perp$). This indicates that the smoke particles are nonabsorbing and that the variation of n with wavelength is small. During the first 2 minutes of the test the refractive index decreases from about 1.39 to about 1.30, which also corresponds to the period of greatest optical density. An average value of $n = 1.36$ was obtained for this period. In addition, it was possible to relax the assumption of nonabsorbing particles and use both the OD_R/OD_B and $I_\parallel/I_\perp$ data simultaneously to calculate values of n and k. An average value of $m = 1.352 - 0.002i$ was obtained by this method, which indicates that the particles are only slightly absorbing.

UNCLASSIFIED

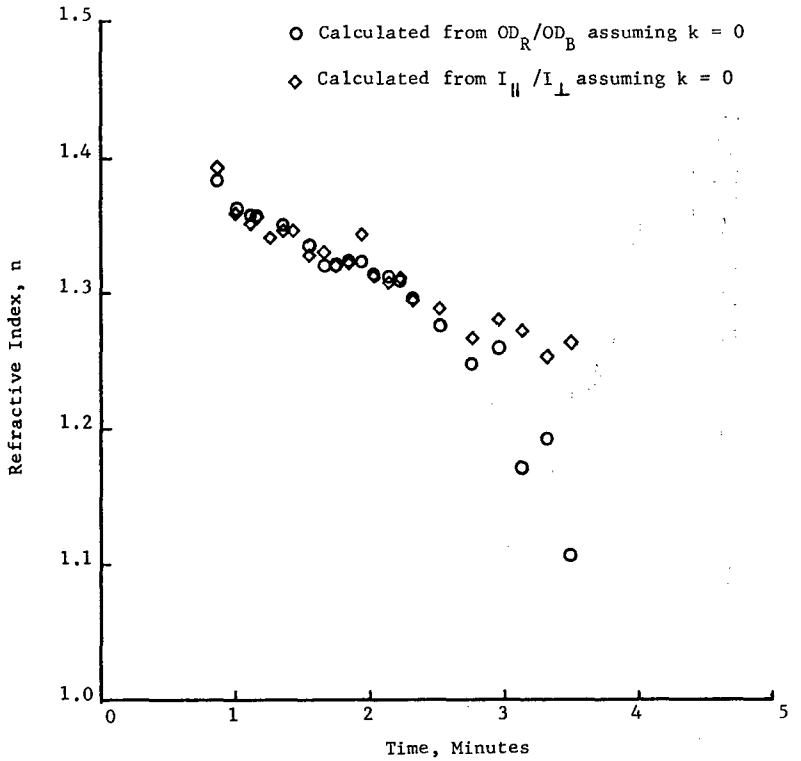

Fig. 15 — Smoke particle refractive index for nonflaming combustion of wall insulation material exposed to a radiant flux of 5 W/cm^2 in room-temperature ventilation air (25°C)

For the test conducted at 100°C the optical density ratio again yielded a refractive index of 1.36. The 90°-scattering ratio, however, indicated a considerably higher value of n (about 1.51). Furthermore it was impossible to find a complex refractive index ($m = n - ik$) which simultaneously fit both the OD_R/OD_B and $I_\parallel/I_\perp$ data. It is therefore likely that the chemical composition of the smoke produced by nonflaming combustion in the 100°C atmosphere differs from that of the room-temperature smoke. The inability to fit the optical density ratio and 90°-scattering data indicates the possibility that the particles are absorbing and that both n and k vary with wavelength. For the 200°C test the concentration of smoke particles was too low for reliable measurements of either OD_R/OD_B or $I_\parallel/I_\perp$; therefore no refractive index data are available for this test.

Calculated particulate volume fractions for the smoldering tests of the wall insulation material are shown in Fig. 16. Due to the unavailability or uncertainty in some of the refractive index values, an assumed value of $m = 1.50 - 0.0i$ was used in obtaining these curves. Somewhat higher volume fractions result if the refractive index data given in Fig. 15 are used in the calculations for the 25°C case. The shapes of the curves of volume fraction versus time and their dependence on temperature are similar to the shapes of the curves of optical density and their dependence on temperature given in Fig. 11. This shows that the optical density of the smoke is determined principally by its concentration and that variations in particle size and refractive index only play secondary roles.

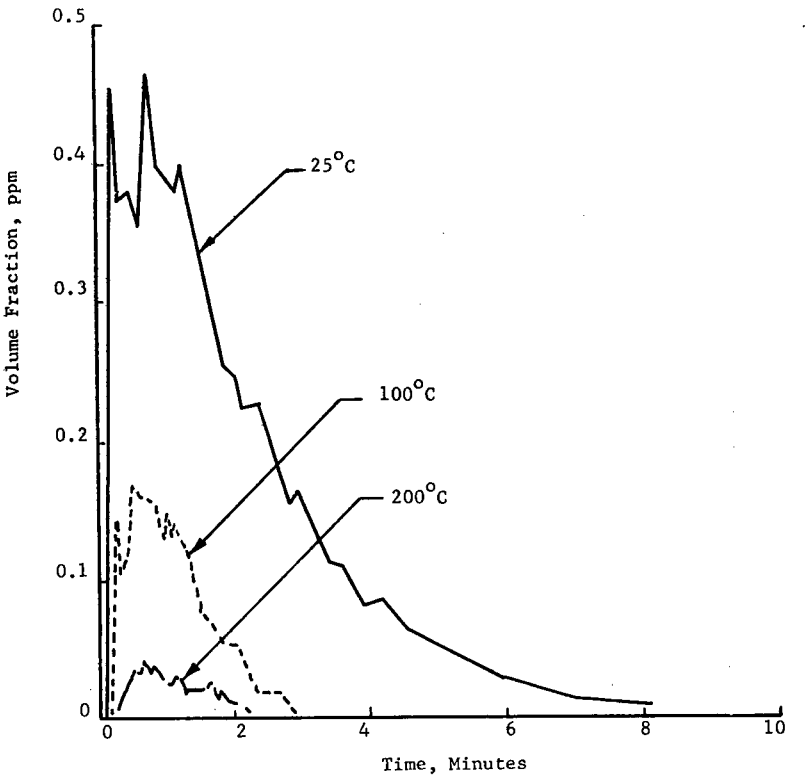

Fig. 16 — Effect of the ventilation air temperature on the particulate volume fraction for nonflaming combustion of wall insulation material exposed to a radiant flux of 5 W/cm^2

For the case of *flaming* combustion of the wall insulation material, the soot particles produced are highly absorbing, and the determination of n and k from the measured values of OD_R/OD_B and $I_\parallel/I_\perp$ is difficult and unreliable. Figure 17 shows values of $I_\parallel/I_\perp$ and OD_R/OD_B plotted as a function of mean particle diameter D_{32} for the room-temperature test. Also plotted in Fig. 17 are curves of $I_\parallel/I_\perp$ and OD_R/OD_B versus D_{32}, which are calculated using the Mie scattering theory. Most of the measured $I_\parallel/I_\perp$ values fall below the theoretical curve for $m = 1.57 - 0.56i$ (Dalzell et al. [10]), and $M = 1.50 - 0.65i$ provides a good fit for the data obtained near the time of peak optical density (between 0.95 and 1.1 μm). On the other hand the measured values of OD_R/OD_B fall well below the Mie curve for soot ($m = 1.57 - 0.56i$) for all values of D_{32} measured. Furthermore it was impossible to fit these data using any other reasonable values of n and k or by assuming reasonable variations of n and k with wavelength. A possible source of the discrepancies in the measured OD_R/OD_B data is the nonspherical shape of the smoke particles. It is well known that sooty smokes consist of large irregular or chainlike agglomerates of smaller soot particles. It is nearly certain that particle shape affects the values of OD_R/OD_B and $I_\parallel/I_\perp$, but in the absence of an adequate scattering theory for nonspherical particles it is not yet possible to calculate the magnitude of the shape effect.

UNCLASSIFIED

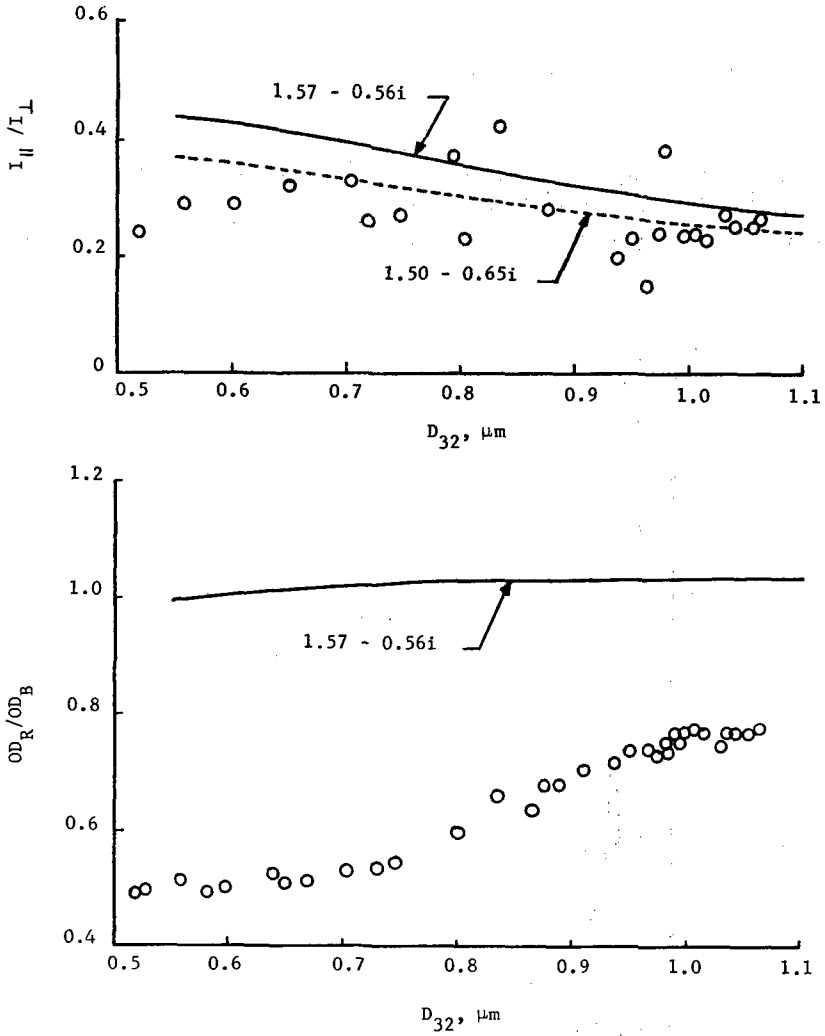

Fig. 17 — Optical density ratios and 90°-scattering ratios for flaming combustion of wall insulation material exposed to a radiant flux of 5 W/cm^2 in room-temperature ventilation air (25°C)

Volume fractions for flaming combustion of the wall insulation material were calculated using $m = 1.57 - 0.56i$ as the refractive index for soot. These curves are presented in Fig. 18 and are corrected to the standard volumetric flow rate of 425 l/min to eliminate the dilution effect at high temperatures. The peak volume fractions are also given in Table 4; these values exhibit the same trend with increasing ambient temperature as the optical density. Again the smoke concentration appears to be the primary factor influencing the light-obscuring properties of the smoke produced by flaming combustion of this material.

Table 4 also shows values of the total particulate volume obtained by integrating the volume fraction curves in Figs. 16 and 18 with respect to time. For nonflaming combustion

the total particulate volume, like the peak volume fraction and the optical density, decreases sharply as the ambient temperature is increased. In contrast, the total particulate volume for flaming combustion is slightly larger at 300°C than at 25°C, and it is least at 100°C. Although no sampling data were available for elevated temperatures, the effect of ambient temperature on Γ was estimated from the optical data. These data are also given in Table 4 for both flaming and nonflaming combustion, where Γ is normalized with respect to the corresponding room-temperature value. The Γ values for both modes of combustion follow the same trends with increasing ventilation air temperature as the total particulate volume.

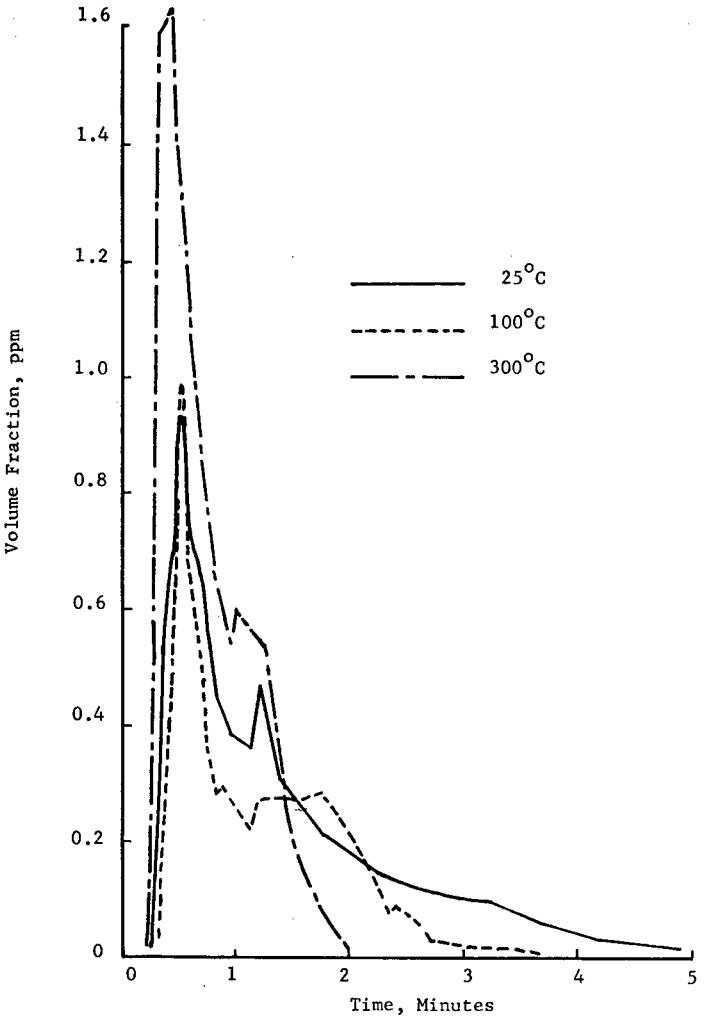

Fig. 18 — Effect of the ventilation air temperature on the particulate volume fraction for flaming combustion of wall insulation material exposed to a radiant flux of 5 W/cm^2

UNCLASSIFIED

Table 4 — Smoke Concentration and Total Volume for Wall Insulation Material

Mode	Ventilation Air Temperature (°C)	Peak Volume Fraction* (ppm)	Total Particulate Volume* (cm^3)	$\frac{\Gamma}{\Gamma_{25}}$
Nonflaming	25	0.46	0.48	1.00
Nonflaming	100	0.17	0.096	0.22
Nonflaming	200	0.042	0.018	0.037
Flaming	25	0.93	0.40	1.00
Flaming	100	0.98	0.28	0.65
Flaming	300	1.63	0.44	1.05

*Based on $m_R = 1.5 - 0.0i$ for nonflaming combustion and $m_R = 1.57 - 0.56i$ for flaming combustion at a standard flow rate of 425 l/min.

With the assumption of a particulate density $\rho_p = 1.3$ g/cm^3 for smoke particles produced by nonflaming combustion and $\rho_p = 2.0$ g/cm^3 for soot produced by flaming combustion, the total particulate mass was estimated from the optically determined total particulate volume. The optically determined values of total particulate mass and Γ were found to be several times greater than the corresponding values estimated by particulate sampling; this factor was about 3.5 for nonflaming combustion and 6.5 for flaming combustion. Possible sources of this discrepancy are losses in the sampling system, departures of the size distribution from that assumed in reducing the optical data, and nonspherical particles (in the case of flaming combustion).

SMOKE PHYSICAL PROPERTIES DATA FOR PVC CABLE JACKET MATERIALS

Two similar polyvinyl chloride (PVC) cable jacket materials were tested under task A. Both were commercially available flexible PVC formulations whose compositions were not available from the manufacturer due to their proprietary nature. The first material tested (PVC-1 cable jacket) was cut into 7.6-cm-long cylindrical sections which had a uniform wall thickness of about 2 mm. To get the sample to lie flat in the horizontal sample mount, it was then cut into four parallel strips. These samples had an exposed surface area of about 58 cm^2, and sample weights were between 16 and 17 g. This material was tested under both flaming and nonflaming combustion in room-temperature ventilation air. The other material (PVC-2 cable jacket) was cut into 3.8-cm sections which had a nonuniform wall thickness varying between 3 and 5 mm. These samples were also cut into four parallel strips, with a total exposed surface area of about 30 cm^2 and sample weights between 15 and 16 g. This material was tested under all conditions specified in Table 1.

Tests in Room-Temperature Ventilation Air

Results of flaming and nonflaming tests of PVC-1 cable jacket in room-temperature atmospheres are presented in Figs. 19 through 22. Results of these tests as well as room temperature data for PVC-2 Cable Jacket are included in Tables 5 and 6.

Sample weight losses for flaming and nonflaming combustion of PVC-1 cable jacket in the 25°C atmosphere are compared in Fig. 19. Here the sample mass loss rates are considerably higher for flaming combustion, but the amount of char residue is about the same in both cases. The presence of a flame has a stronger effect for PVC-2 cable jacket, with the peak mass loss rate for flaming combustion being over 3 times the maximum mass loss rate obtained for nonflaming combustion (Table 5). PVC-2 cable jacket also leaves considerably more char residue than the PVC-1 material under both nonflaming and flaming conditions.

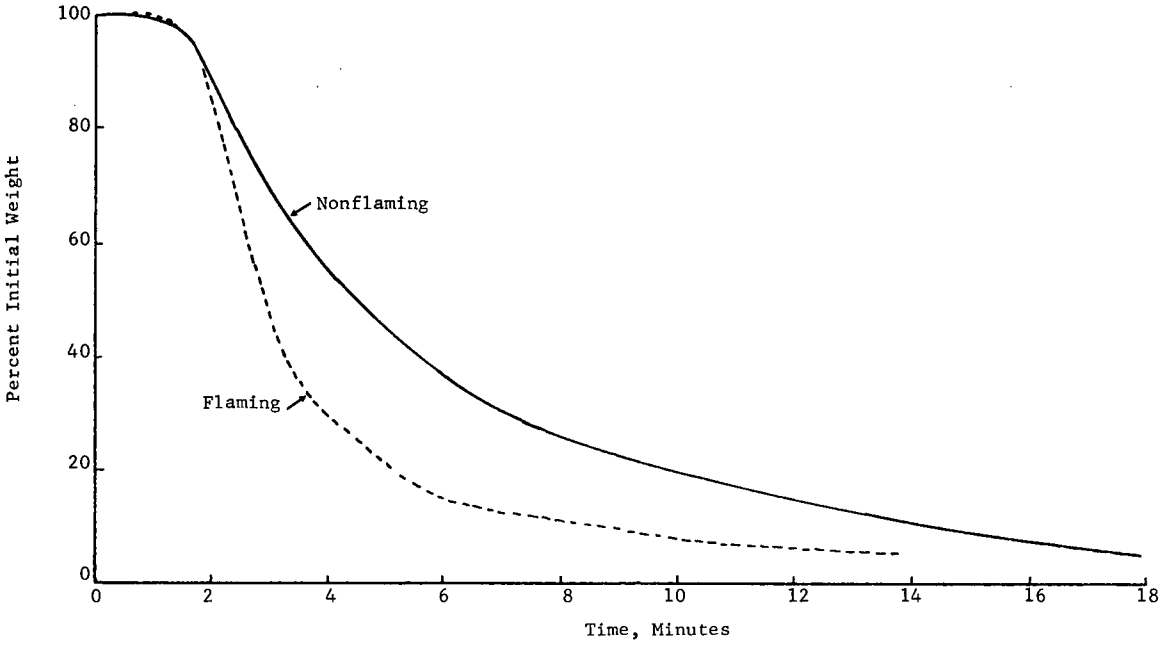

Fig. 19 — Sample weight losses for flaming and nonflaming combustion of PVC-1 cable jacket exposed to a radiant flux of 5 W/cm^2 in room-temperature ventilation air (25°C)

UNCLASSIFIED

Table 5 — Sample Weight Loss Data for PVC Cable Jacket Materials

PVC	Mode	Ventilation Air Temperature (°C)	Peak Mass Loss Rate (mg/cm^2-s)	Char Residue (% of Initial Weight)
1	Nonflaming	25	1.07	3.8
1	Flaming	25	1.78	5.4
2	Nonflaming	25	0.94	25
2	Nonflaming	100	0.83	24
2	Nonflaming	200	1.40	18
2	Flaming	25	3.20	16
2	Flaming	100	2.03	13
2	Flaming	300	2.73	10

Table 6 — Smoke Properties Data for PVC Cable Jacket Materials

PVC	Mode	Ventilation Air Temperature (°C)	Γ	D_{MMD} (μm)	σ_g	OD_{max}		D_{32}* (μm)	Time to Peak OD (min)
						Blue	Red		
1	Nonflaming	25	0.083	1.61	2.33	1.92	1.77	1.18	4.6
2	Nonflaming	25	—	—	—	1.07	1.12	0.99	3.1
2	Nonflaming	100	—	—	—	1.01	0.92	0.85	3.4
2	Nonflaming	200	—	—	—	0.74	0.50	0.76	3.8
1	Flaming	25	1.026	0.79	4.07	6.02	4.55	1.11	2.6
2	Flaming	25	—	—	—	5.14	3.93	1.01	2.2
2	Flaming	100	—	—	—	4.96	3.86	1.08	2.1
2	Flaming	300	—	—	—	4.75	3.75	1.13	1.3

*Average for data points near the time of maximum optical density.

Smoke particle size distributions for flaming and nonflaming combustion of PVC-1 cable jacket are presented in Fig. 20. For flaming combustion the cascade impactor data fall close to a straight line, indicating a log-normal distribution, and for nonflaming combustion the data depart from the log-normal distribution for particle diameters greater than 3 μm (about 20% of the total particulate mass). Mass median diameters (D_{MMD}) and standard deviations (σ_g) obtained from these curves are given in Table 6. Like the wall insulation material, the PVC-1 cable jacket produced particles during flaming combustion that have a smaller mass median diameter and a larger standard deviation than those it produced during nonflaming conditions. Comparison in Table 3 also shows that the PVC-1 cable jacket produces smoke particles with a D_{MMD} 2 to 3 times larger than those produced by the wall insulation material. Samples of smoke particulates collected during nonflaming tests of PVC-1 cable jacket consisted of a yellowish, tarry liquid, and those obtained during the flaming tests were predominantly sooty. The fraction of the total mass loss which is converted to particulates (Γ) is also given in Table 6 for PVC-1. For this material Γ values for nonflaming combustion are about 3 times larger than those for flaming combustion.

Mean particle diameters D_{32} obtained with the in situ optical system are given in Fig. 21 for PVC-1 cable jacket. For nonflaming combustion a sharp peak in D_{32} exceeding 1.4 μm occurs early in the test, before the period of maximum optical density, which is then followed by a decline in D_{32} to about 0.8 μm after 12 minutes. For flaming combustion a lower, broader D_{32} peak of about 1.1 μm occurs simultaneously with the maximum in optical density. The characteristic value of D_{32} at peak optical density (Table 6) for PVC-1 cable jacket is between 1.1 and 1.2 μm for both smoldering and flaming combustion. For nonflaming combustion the mass median diameter D_{MMD} obtained from the collected samples is considerably larger than the D_{32} value obtained optically, whereas D_{32} is greater than D_{MMD} in the flaming case. Similar differences in D_{MMD} and D_{32} were also obtained for flaming combustion of the wall insulation material. Such differences in the two mean particle diameters probably arise from the same causes noted earlier for the wall insulation material.

Optical density variations during flaming and nonflaming tests of the PCV-1 cable jacket are given in Fig. 22. For smoldering combustion a broad optical density peak of about 2.0 m^{-1} occurs about 5 minutes after exposure of the sample to the 5-W/cm^2 radiant flux. For flaming combustion, the additional radiant heat flux from the flame results in a greater sample mass loss rate and a much greater peak optical density of about 6.0 m^{-1}. The peak in optical density is also much sharper and occurs earlier during flaming combustion.

Differences and similarities were also observed in the smoking behavior of the two PVC cable jacket materials tested. For smoldering combustion the PVC-2 cable jacket material also exhibits a sharp D_{32} peak of about 1.5 μm which occurs before the maximum in optical density (Fig. 24). The peak optical density for PVC-2 is about 1/2 that obtained with the PVC-1 material under nonflaming conditions, and the characteristic D_{32} value is only slightly smaller. Under flaming combustion PVC-2 cable jacket exhibits a somewhat smaller peak optical density and a smaller corresponding mean particle diameter than PVC-1 (Table 6). Maximum mass loss rates for the two PVC formulations are about the same for smoldering combustion, but PVC-2 yields considerably higher mass loss rates than PVC-1 for flaming combustion.

UNCLASSIFIED

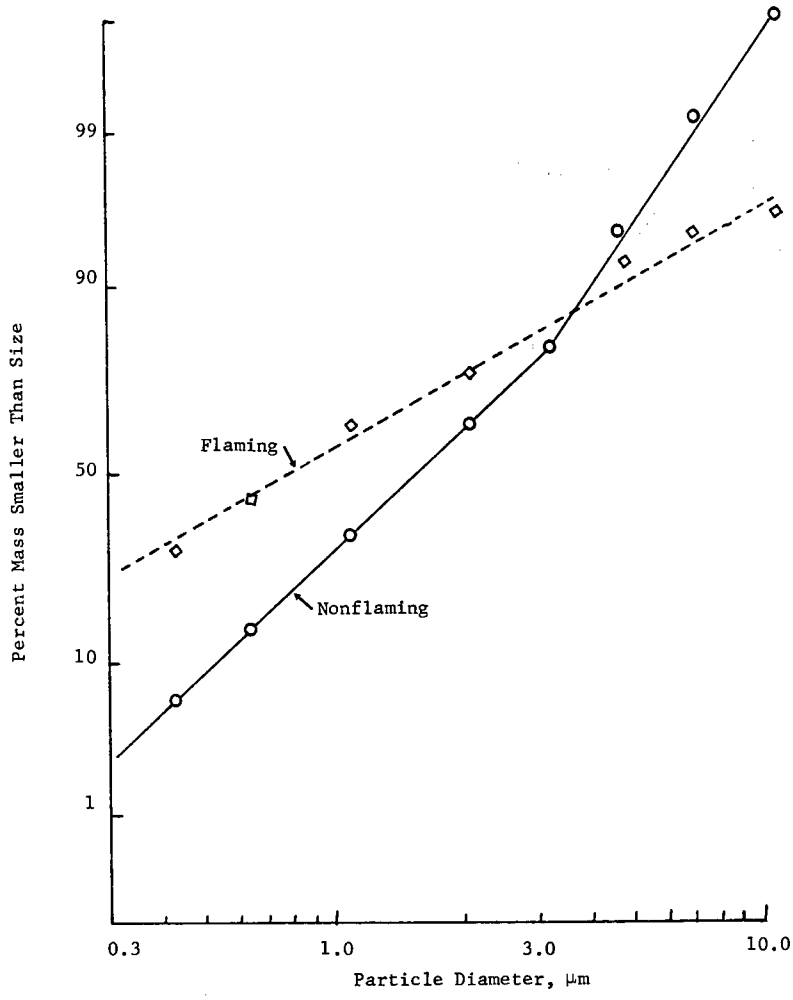

Fig. 20 — Smoke particle size distributions for flaming and nonflaming combustion of PVC-1 cable jacket exposed to a radiant flux of 5 W/cm^2 in room-temperature ventilation air (25°C)

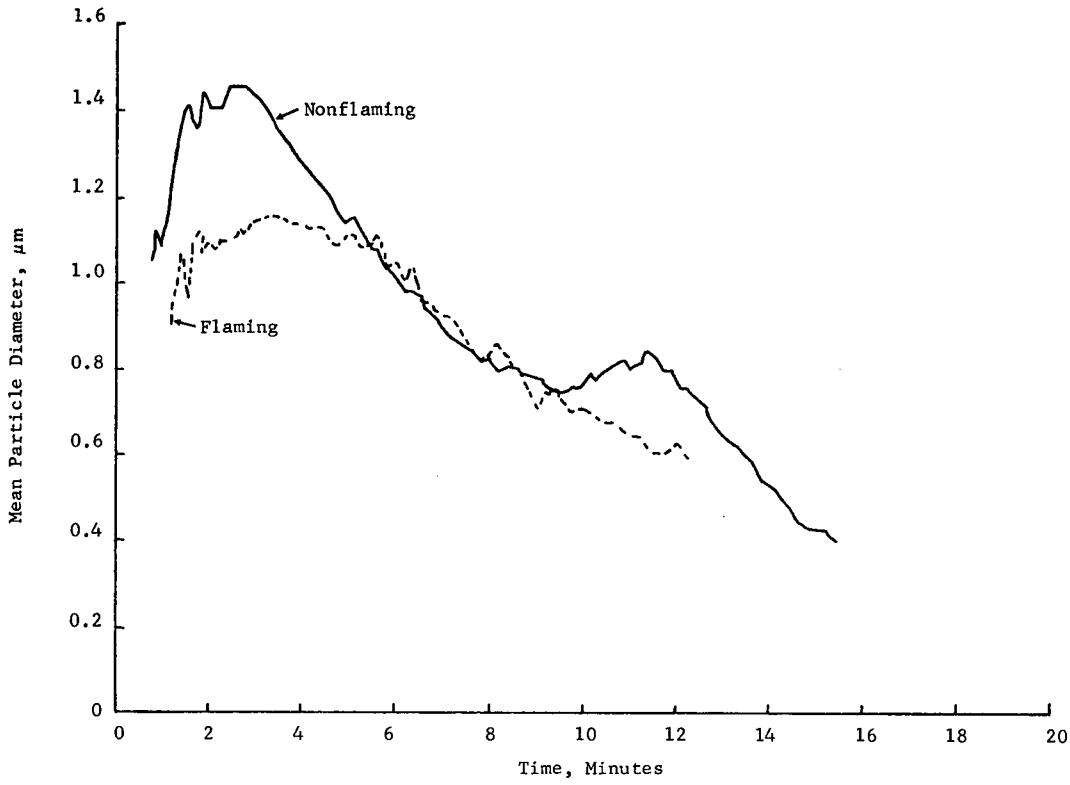

Fig. 21 — Smoke mean particle diameters for flaming and nonflaming combustion of PVC-1 cable jacket exposed to a radiant flux of 5 W/cm^2 in room-temperature ventilation air

UNCLASSIFIED

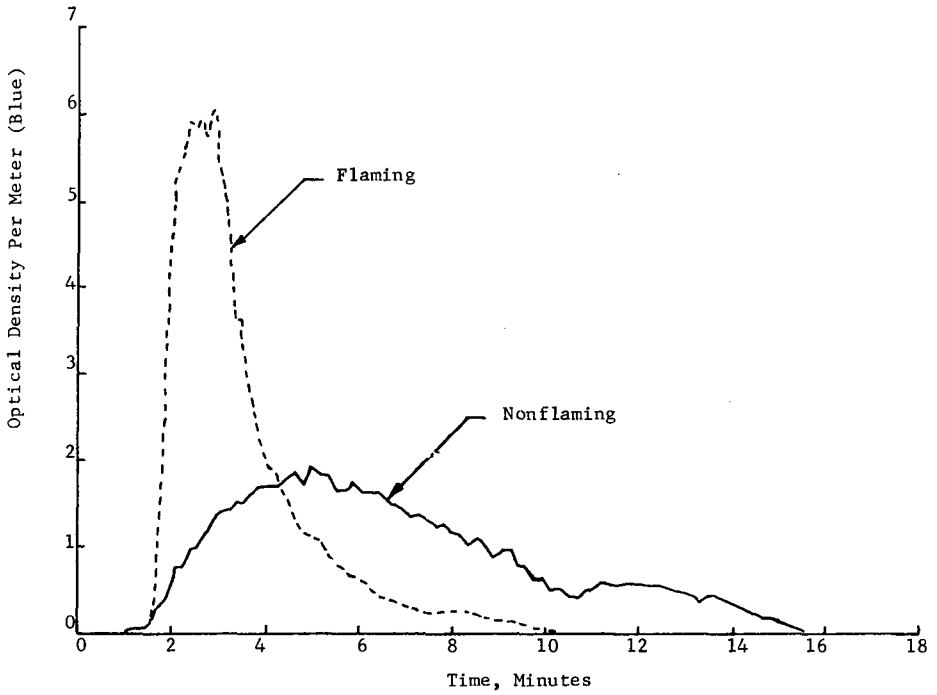

Fig. 22 — Smoke optical densities for flaming and nonflaming combustion of PVC-1 cable jacket exposed to a radiant flux of 5 W/cm^2 in room temperature ventilation air (25°C)

Tests in Heated Ventilation Air

Results of tests of the PVC-2 cable jacket in heated ventilation air are presented in Figs. 23 through 25 for smoldering combustion and in Figs. 26 through 28 for flaming combustion. In each of these plots the room-temperature data for the same material are shown for comparison. High-temperature data for the PVC-2 cable jacket are also given in Tables 5 and 6. As shown in Table 1, nonflaming tests were conducted at ventilation air temperatures of 100°C and 200°C, since flaming ignition occurred at 300°C. Flaming data were obtained at 100°C and 300°C.

Figure 23 and Table 5 shows that for *nonflaming* combustion of the PVC-2 cable jacket, heating the ventilation air to 100°C has little effect on the sample mass loss rate (just under 1.0 mg/cm^2-s) and the amount of char residue (about 25% of the initial sample weight). Further heating of the ventilation air to 200°C results in a moderate increase in the peak sample mass loss rate and a corresponding decrease in the amount of char residue. At ambient temperatures above 300°C, radiant exposure to 5 W/cm^2 results in flaming ignition of the sample after about 30 seconds.

Plots of mean particle diameter D_{32} versus time given in Fig. 24 show that the initial D_{32} peak is increasingly suppressed as the ambient temperature is increased for smoldering combustion of the PVC-2 cable jacket. Thus this peak is probably due to pyrolysis products

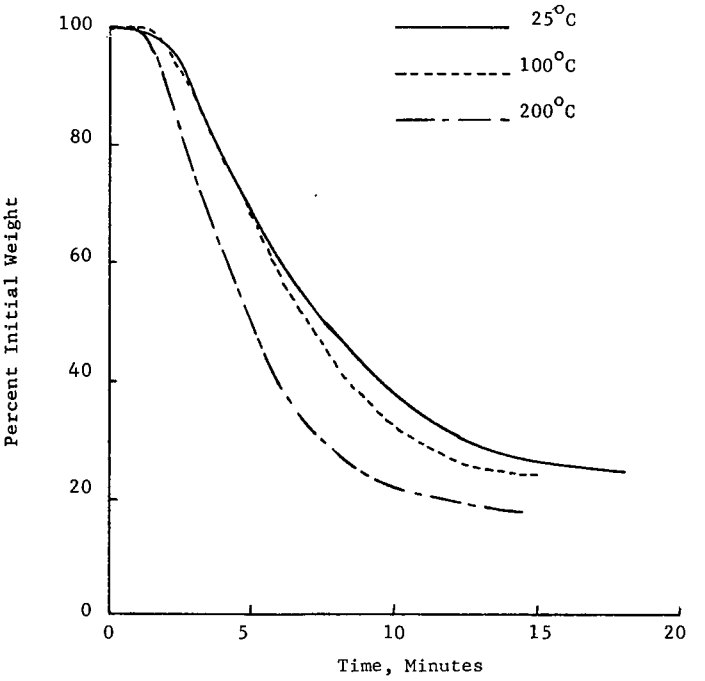

Fig. 23 — Effect of the ventilation air temperature on the sample weight loss for nonflaming combustion of PVC-2 cable jacket exposed to a radiant flux of 5 W/cm^2

with lower boiling points (below 200°C) which are evolved early in the test and do not condense in the higher temperature environment. The D_{32} plots in Fig. 24 and the characteristic mean particle diameters corresponding to maximum optical density in Table 6 reveal a small but steady decrease in mean particle size as the ventilation air temperature is increased from room temperature to 200°C. The ambient temperature had a similar effect upon D_{32} for the wall insulation material. Typical mean particle diameters measured for the PVC-2 cable jacket in this temperature range lie between 0.7 and 1.0 μm.

Figure 25 shows that the smoldering PVC-2 cable jacket exhibits a trend of decreasing optical density as the ambient temperature is increased. Most of this decrease, however, is due to the increased dilution resulting from the higher volumetric flow rate of the heated ventilation air. When this effect is removed, as in the peak optical densities given in Table 6, increasing the environmental temperature to 200°C reduces the optical density in blue light by only about 30%. This is in strong contrast to the results given earlier for the wall insulation material, for which optical densities were reduced by an order of magnitude by the same ambient temperature increases. Thus the mechanism of smoke production for nonflaming combustion of the PVC-2 cable jacket is much less sensitive to ambient temperature than for the wall insulation material. This may indicate that the pyrolysis products generated by the PVC-2 material generally have higher boiling points than those produced by the wall insulation material.

UNCLASSIFIED

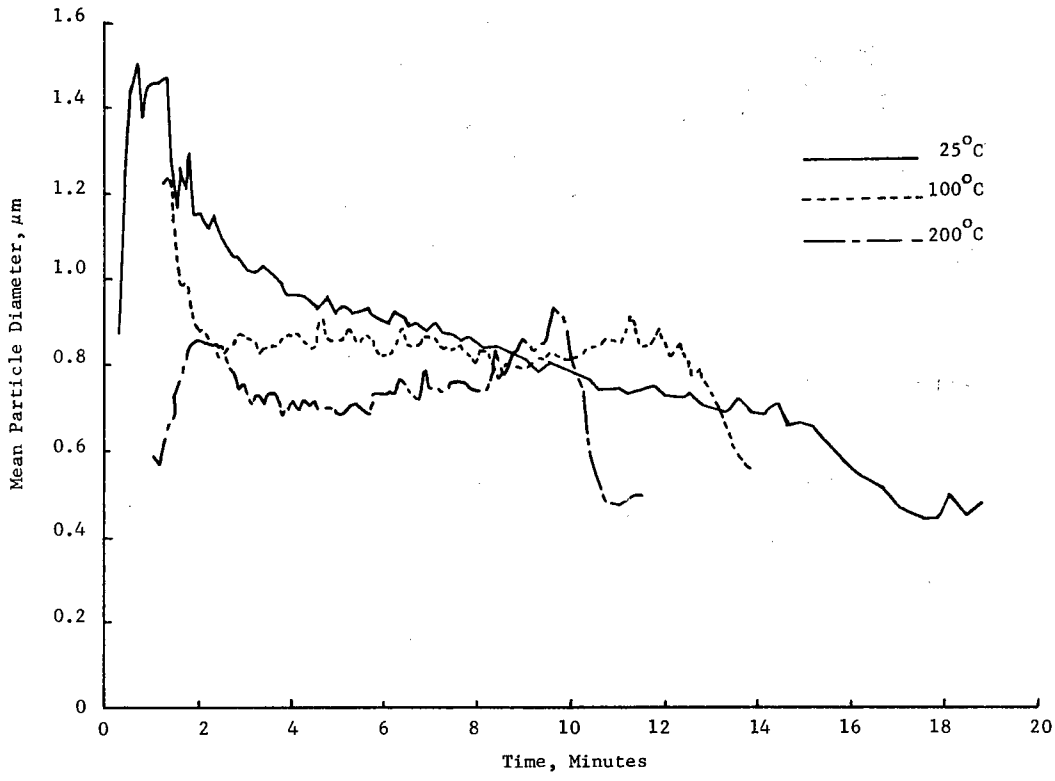

Fig. 24 — Effect of the ventilation air temperature on the smoke mean particle diameter for nonflaming combustion of PVC-2 cable jacket exposed to a radiant flux of 5 W/cm^2

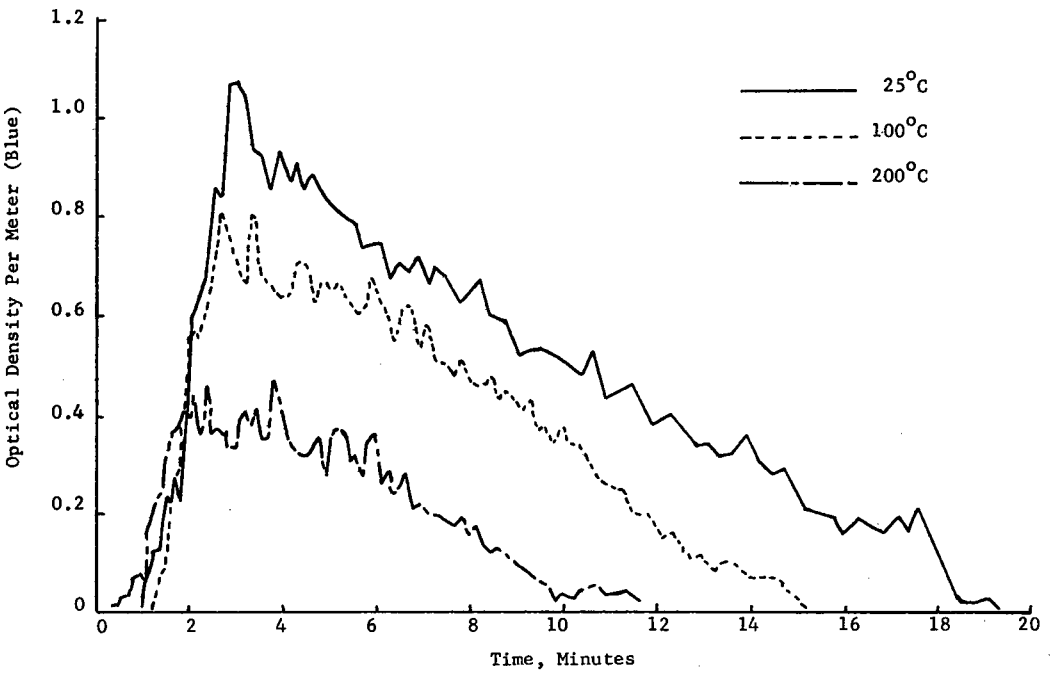

Fig. 25 — Effect of the ventilation air temperature on the smoke optical density for nonflaming combustion of PVC-2 cable jacket exposed to a radiant flux of 5 W/cm^2

The effect of ambient temperature on sample weight loss for *flaming* tests of the PVC-2 cable jacket is shown in Fig. 26. These curves and the data in Table 5 show that environmental temperature has little effect upon PVC-2 mass loss rates under flaming conditions, but the onset of pyrolysis occurs much earlier at 300°C than at temperatures below 100°C. Also the amount of char residue is significantly reduced as the environmental temperature is increased; less than 1/2 as much char is produced under flaming combustion in 300°C air than under nonflaming conditions in room-temperature air.

Figure 27 shows that in flaming tests of PVC-2 cable jacket the mean particle diameter D_{32} is nearly constant throughout most of the test for each ambient temperature considered. Increasing the air temperature to 100°C results in a small increase in D_{32}, but a further increase to 300°C has little effect on D_{32}. The characteristic values of D_{32} corresponding to maximum optical density (Table 6) also show only a small increase in mean particle diameter with increasing ambient temperature. Thus the PVC-2 cable jacket material produces particles with a mean diameter between 1.0 and 1.2 μm during flaming combustion in air at temperatures between 25°C and 300°C.

Optical densities for flaming combustion of PVC-2 cable jacket are shown in Fig. 28. Again most of the observed decrease in optical density with increasing ambient temperature is due to the higher flow rate of the heated air. The corrected values of peak optical density given in Table 6 show that increasing the ventilation air temperature to 300°C results in only a small decrease in maximum optical density (less than 10%). The earlier occurrence

UNCLASSIFIED

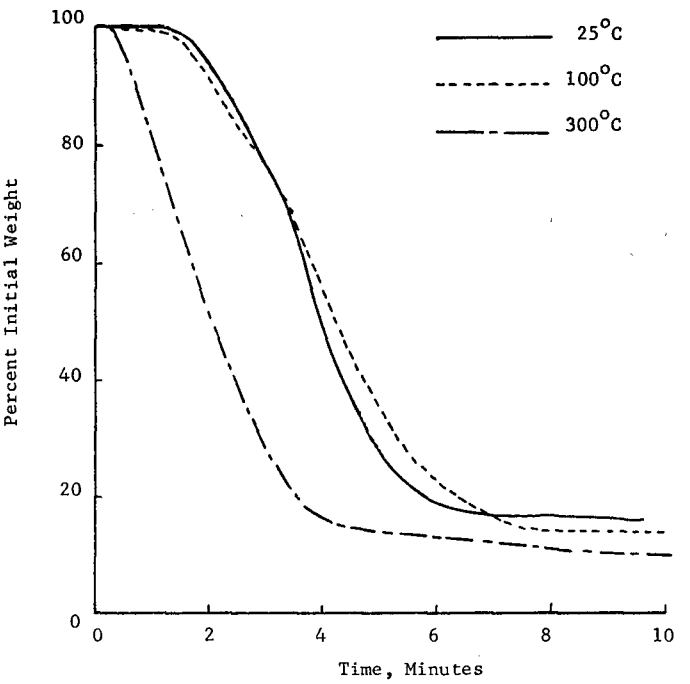

Fig. 26 — Effect of the ventilation air temperature on the sample weight loss for flaming combustion of PVC-2 cable jacket exposed to a radiant flux of 5 W/cm^2

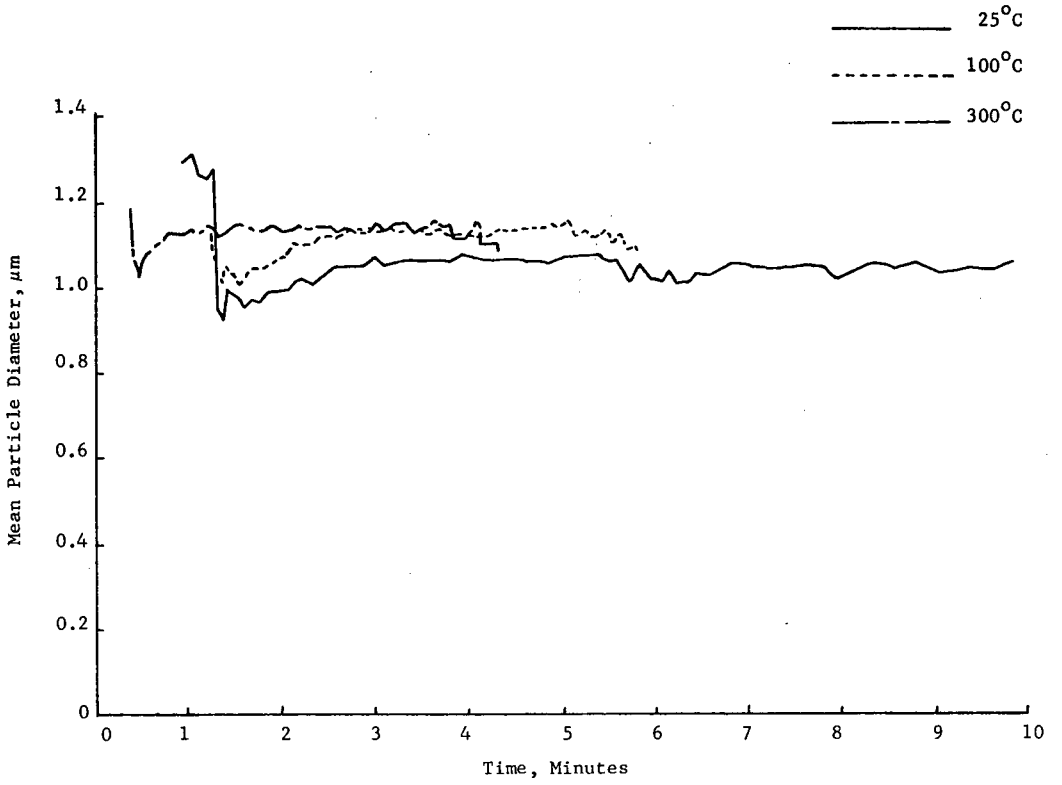

Fig. 27 — Effect of the ventilation air temperature on the smoke mean particle diameter for flaming combustion of PVC-2 cable jacket exposed to a radiant flux of 5 W/cm^2

UNCLASSIFIED

of the peak optical density at 300°C corresponds with the earlier onset of sample mass loss noted previously.

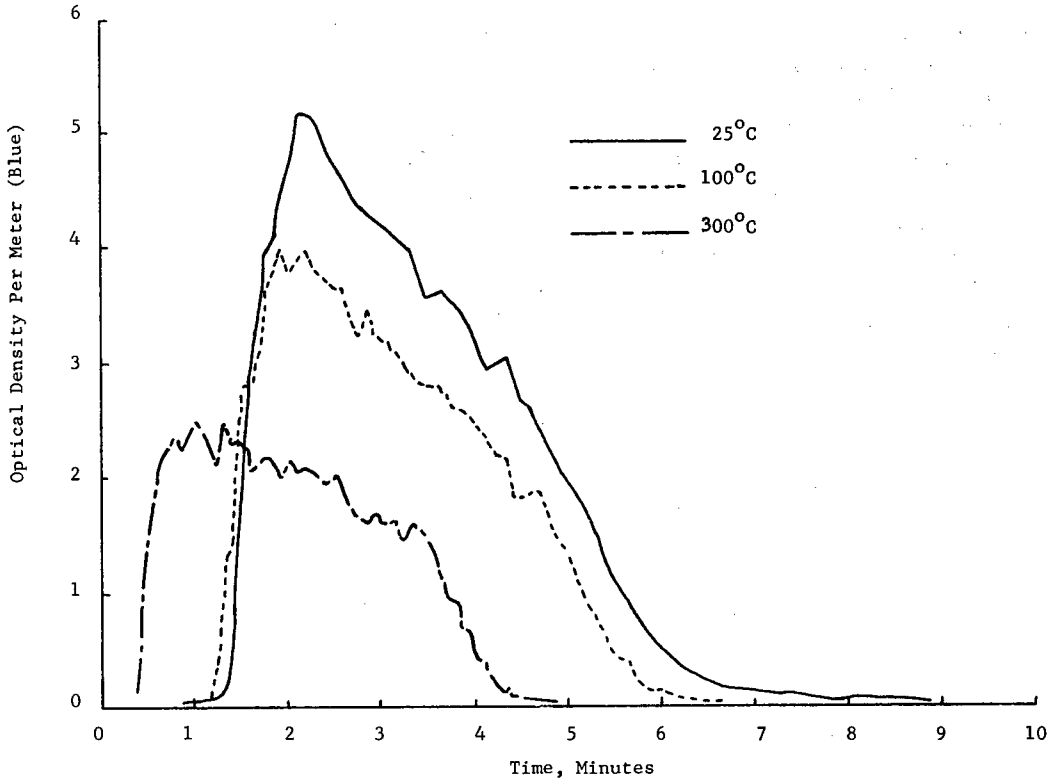

Fig. 28 — Effect of the ventilation air temperature on the smoke optical density for flaming combustion of PVC-2 cable jacket exposed to a radiant flux of 5 W/cm^2

The data presented above indicate that smoke characteristics for PVC-2 cable jacket are relatively insensitive to ambient temperature, especially for flaming combustion. Unlike the wall insulation material, heating the ventilation air does not lead to more fuel-rich burning for PVC-2, because the pyrolysis rate (mass loss rate) does not increase.

Smoke Particle Refractive Index and Volume Fraction

Several methods were used to determine values of the refractive index of the smoke particles produced during *nonflaming* tests of both PVC cable jacket materials. With the assumption that the smoke particles were nonabsorbing ($k = 0$), values of the refractive index n were obtained from the optical density ratio (OD_R/OD_B) and the 90°-scattering ratio ($I_\parallel/I_\perp$). As seen from Table 7, the refractive index calculated from $I_\parallel/I_\perp$ is always larger than the refractive index computed from OD_R/OD_B. Next, the assumption of $k = 0$ was relaxed, but the complex refractive index $m = n - ik$ was assumed to be independent of wavelength. Except for a small number of data points for PVC-1 at 25°C, no solutions were found which satisfied both the measured OD_R/OD_B and $I_\parallel/I_\perp$ values under this assumption. Finally, plots of OD_R/OD_B and $I_\parallel/I_\perp$ as a function of mean particle size D_{32} were constructed. These plots are given in Fig. 29 for PVC-1 and in Fig. 30 for PVC-2. Various values of the complex refractive index at the two wavelengths (m_R and m_B) were assumed until a reasonably good curve fit was obtained for the data points near the time of maximum optical density. The resulting values of m_R and m_B are given in Table 7, and the corresponding theoretical curves of OD_R/OD_B and $I_\parallel/I_\perp$ versus D_{32} are also plotted in Figs. 29 and 30. These values are not unique, as there are more unknown quantities (n_R, k_R, n_B, and k_B) than there are restraints (OD_R/OD_B, and $I_\parallel/I_\perp$). Nevertheless these results indicate some general optical characteristics of the smoke particles produced by these PVC materials under nonflaming conditions. Both PVC-1 and PVC-2 smoke particles appear to have greater refractive indices n in red light ($\lambda = 633$ nm) than in blue light ($\lambda = 458$ nm). The PVC-1 smoke particles seem to be moderately absorbing in red light ($k \approx 0.1$) and only slightly absorbing ($k \approx 0.01$) in blue light. In contrast the PVC-2 smoke particles are somewhat more absorbing in blue light than in red light.

Table 7 — Smoke Refractive Indices for PVC Cable Jacket Materials

PVC	Mode	Ventilation Air Temperature (°C)	Refractive Index*		Curve Fit ($m_R \neq m_B$)	
			$k = 0$ From OD_R/OD_B	$m_R = m_B$ From $I_\parallel/I_\perp$	m_R	m_B
1	Nonflaming	25	1.28	1.34	$1.54 - 0.11i$	$1.33 - 0.01i$
2	Nonflaming	25	1.39	1.60	$1.60 - 0.05i$	$1.35 - 0.08i$
2	Nonflaming	100	1.37	1.42	$1.53 - 0.09i$	$1.36 - 0.00i$

*Averages for data points near the time of maximum optical density.

For *flaming* combustion of the PVC-1 cable jacket, values of $I_\parallel/I_\perp$ obtained near the time of maximum optical density are in good agreement with theoretical values obtained with the complex refractive index of soot, $m = 1.57 - 0.56i$. As in the case of the wall insulation material, measured values of OD_R/OD_B are about 20% below the Mie curve for soot for the values of D_{32} measured. Also it was not possible to fit these data with other reasonable choices of m_R and m_B. Again it appears that nonspherical smoke particles may account for this discrepancy in the measured and theoretical values of OD_R/OD_B.

UNCLASSIFIED

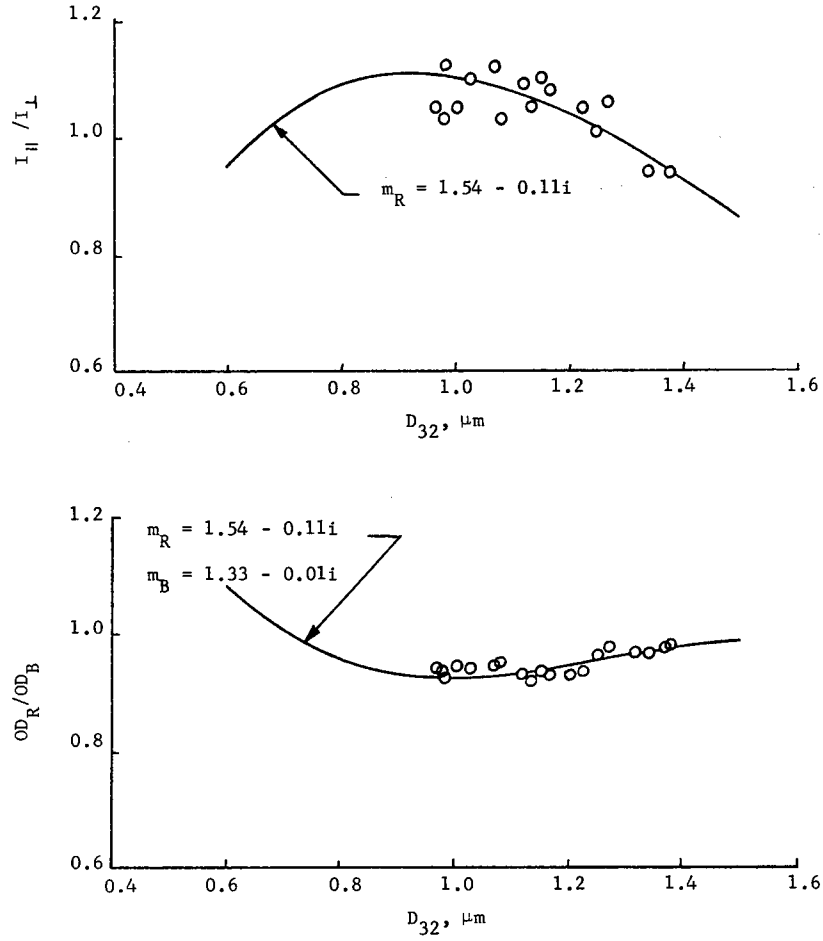

Fig. 29 — Optical density ratios and 90°-scattering ratios for nonflaming combustion of PVC-1 cable jacket exposed to a radiant flux of 5 W/cm^2 in room-temperature ventilation air (25°C)

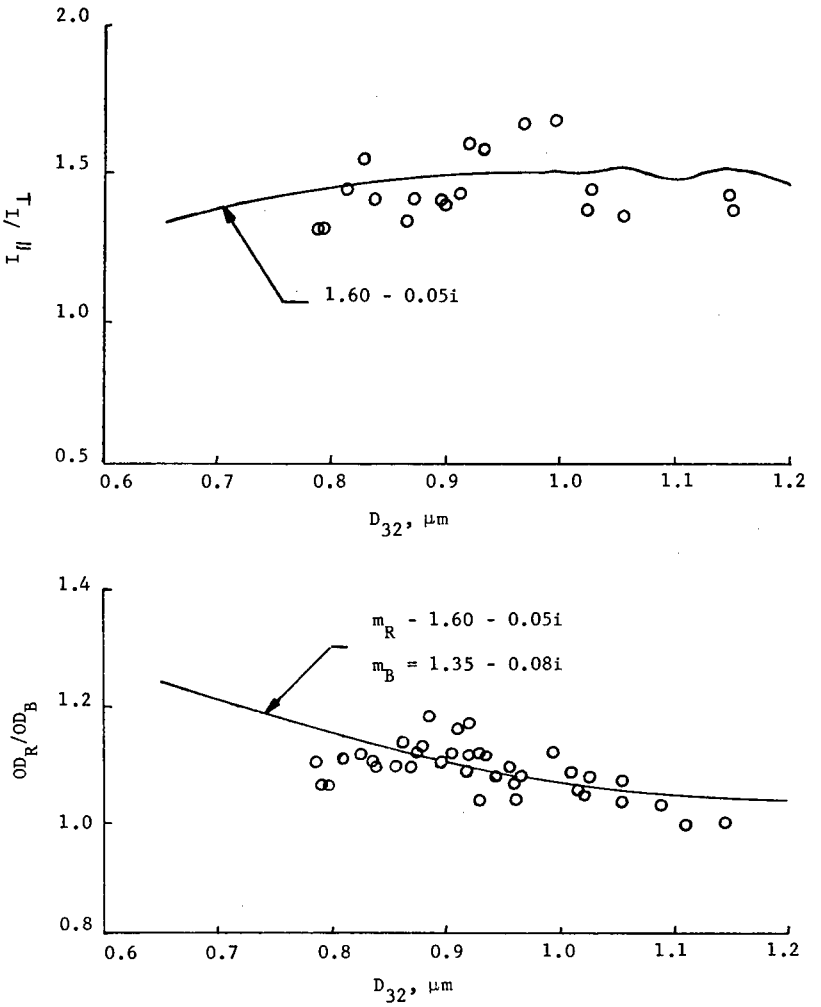

Fig. 30 — Optical density ratios and 90°-scattering ratios for nonflaming combustion of PVC-2 cable jacket exposed to a radiant flux of 5 W/cm^2 in room-temperature ventilation air (25°C)

UNCLASSIFIED

Curves of smoke particle volume fraction versus time are shown in Fig. 31 for smoldering combustion of the PVC-2 cable jacket. Similar curves for flaming combustion are shown in Fig. 32. Table 8 gives peak volume fractions, total particulate volumes, and relative Γ values which were obtained from these data. All of these data (Figs. 31 and 32 and Table 8) have been corrected to eliminate the effect of increased dilution at elevated ambient temperatures.

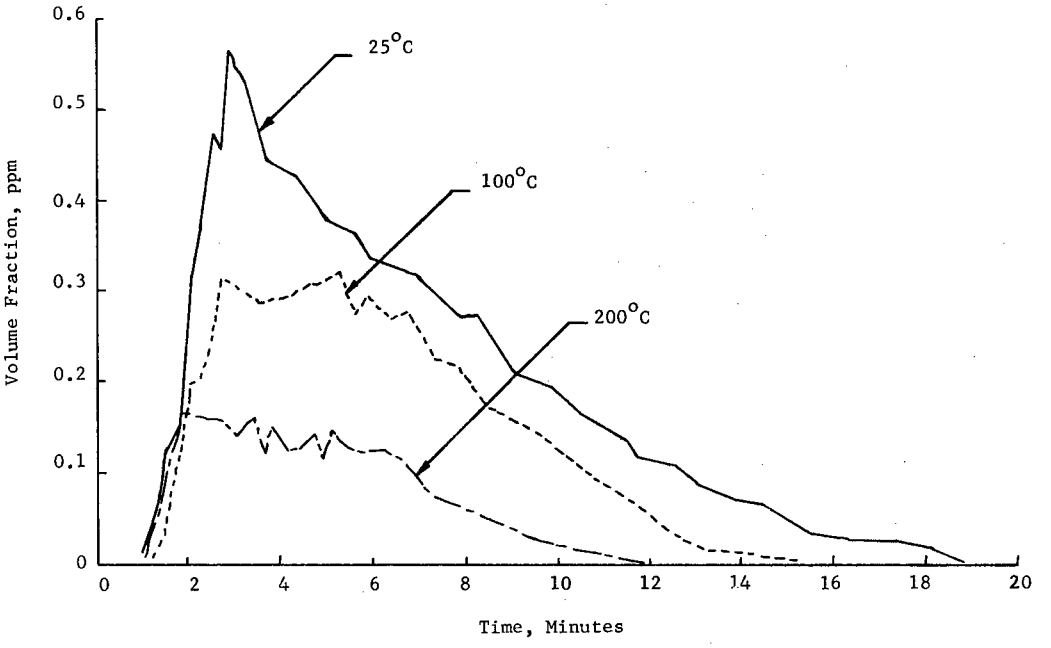

Fig. 31 — Effect of the ventilation air temperature on the particulate volume fraction for nonflaming combustion of PVC-2 cable jacket exposed to a radiant flux of 5 W/cm^2

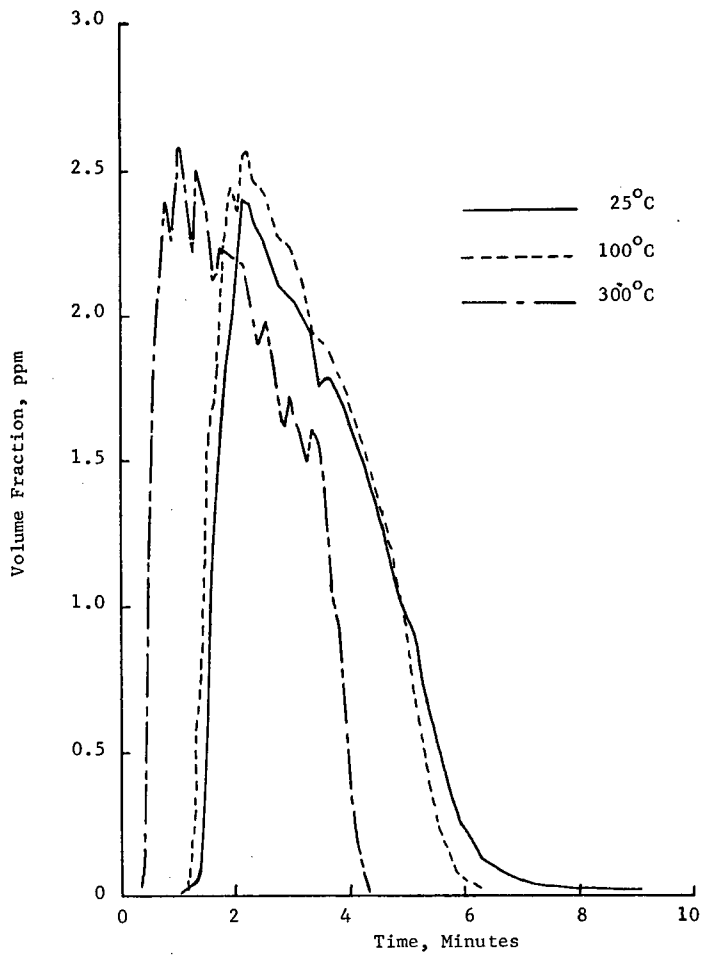

Fig. 32 — Effect of the ventilation air temperature on the particulate volume fraction for flaming combustion of PVC-2 cable jacket exposed to a radiant flux of 5 W/cm^2

UNCLASSIFIED

Table 8 — Smoke Concentration and Total Volume for PVC Cable Jacket Materials

PVC	Mode	Ventilation Air Temperature (°C)	Peak Volume Fraction* (ppm)	Total Particulate Volume* (cm^3)	$\frac{\Gamma}{\Gamma_{25}}$
1	Nonflaming	25	1.14	2.68	—
1	Flaming	25	3.13	2.84	—
2	Nonflaming	25	0.56	1.49	100
2	Nonflaming	100	0.32	0.96	0.65
2	Nonflaming	200	0.16	0.40	0.24
2	Flaming	25	2.40	2.95	1.00
2	Flaming	100	2.57	3.08	1.05
2	Flaming	300	2.58	2.85	0.90

*Based on m_R 1.50 - 0.0i for nonflaming combustion and m_R = 1.57 - 0.56i for flaming combustion at a standard flow rate of 425 l/min.

The data in Fig. 31 for nonflaming combustion and the corresponding data in Table 8 were calculated assuming a refractive index of m_R = 1.5 - 0.0i. Using the curve fit value of m_R = 1.60 - 0.05i yielded volume fractions only about 10% higher. These results show that the volume fraction curves, peak volume fraction, total particulate volume, and relative Γ values all decrease with increasing ambient temperature for nonflaming combustion of the PVC-2 cable jacket. The effect of ambient temperature on these quantities is stronger than the corresponding effect on optical density given in Table 6. Peak volume fraction and total particulate volume were also calculated for the PVC-1 cable jacket; these values are about twice as large as the corresponding data for PVC-2. This is consistent with the larger optical densities obtained during nonflaming tests of the PVC-1 material.

The particulate volume fractions for flaming tests of the PVC-2 cable jacket given in Fig. 32 were calculated using the soot refractive index m_R = 1.57 - 0.056i. Like the optical density, ventilation air temperature has little effect on the magnitude of the volume fractions for flaming PVC-2, although the peak occurs earlier at the highest temperature. Also environmental temperature has little effect on the total particulate volume or the fraction of the total mass loss converted to particulates (Γ) under flaming conditions. Table 8 also gives flaming data for the PVC-1 cable jacket. The PVC-1 material yields a somewhat higher peak volume fraction than the PVC-2 material, but the total particulate volume is about the same for both PVC materials.

The total particulate mass was also estimated from the total particulate volume by assuming a particulate density ρ_p = 1/3 g/cm^3 for nonflaming combustion and ρ_p = 2.0 g/cm^3 for flaming combustion. Optically determined values of the total particulate mass for the PVC-1 cable jacket were then compared with the corresponding values obtained by particulate sampling. For smoldering combustion the optically determined particulate mass was about 2.5 times greater than the particulate mass obtained by

sampling, and the corresponding factor was nearly 12 for the case of flaming combustion. Similar discrepancies were noted earlier for the wall insulation material, and the same causes are probably responsible for these discrepancies in the present case. More specifically, the order-of-magnitude discrepancy in the total particulate masses as determined by the optical and sampling techniques for flaming combustion probably indicates that the soot particles are highly nonspherical. These results are consistent with previous electron microscope results which show smoke particles to consist of chainlike agglomerates of smaller spherical soot particles.

SMOKE PHYSICAL PROPERTIES DATA FOR HYDRAULIC FLUID

Samples of the hydraulic fluid (2190 TEP, MIL-L-17331A) were tested under task A. For each test 20 g of the hydraulic fluid was placed in a shallow circular aluminum dish (about 7.6 cm in diameter and 1 cm deep), which was mounted in the CPTC. The exposed surface area of these samples was approximately 45 cm^2.

Tests in Room-Temperature Ventilation Air

The hydraulic fluid was the most flammable of the materials tested; thus only a limited number of nonflaming data were obtained. Nonflaming conditions were maintained during only the first 6 minutes after exposure of the hydraulic fluid to the 5-W/cm^2 radiant flux in the room-temperature environment. During this period of heating, evaporation, and pyrolysis of the liquid material only about 5% of the original sample mass was lost. Some of the vapors condensed to form smoke particles whose mean diameters D_{32} ranged between 1.0 and 1.5 μm. A peak mass loss rate of about 0.14 mg/cm^2-s and a maximum optical density of about 1.2 m^{-1} occurred just before flaming ignition at 5.9 minutes. The mean particle diameter at the time of peak optical density during the nonflaming phase was a little over 1.2 μm. After flaming ignition D_{32} rose to a nearly constant value of 1.3 μm and the optical density peaked at nearly 7.0 m^{-1} at 8.6 minutes. Weight loss was rapid during flaming combustion, approaching 6 mg/cm^2-s, and the sample was entirely consumed after 10 minutes.

An additional room-temperature test was conducted in which flaming combustion was initiated earlier using the propane pilot flame. Plots of weight loss, mean particle diameter D_{32}, and optical density for this test are given in Figs. 33, 34, and 35 respectively, along with the corresponding high-temperature data. Even with the pilot flame, during an initial nonflaming phase the concentration of combustible vapors increases until the flammability limit is reached. Again a peak optical density of about 7.0 m^{-1} and mean particle diameters of about 1.3 μm are obtained during flaming combustion. Cascade impactor samples collected during this test revealed large quantities of fluffy black soot aggregates on all stages. Many of the larger soot particles did not adhere to the upper cascade impactor plates but were carried below, where they clogged the holes in the lower stages. Thus the cascade impactor data for flaming tests of the hydraulic fluid are unreliable, and no particle size distributions, mass median diameters, or standard deviations are available for this material. Another test was conducted with two filters in series substituted for the cascade impactor. In this test about 37 mg of soot was collected, yielding a Γ value of about 0.028.

UNCLASSIFIED

Tests in Heated Ventilation Air

Due to the occurrence of spontaneous ignition in room-temperature tests of the hydraulic fluid, no *nonflaming* tests were attempted at higher environmental temperatures. Flaming tests of the hydraulic fluid were conducted using the pilot flame for ventilation air temperatures of 100°C and 300°C. These results are compared with the corresponding room-temperature results in Figs. 33 through 35 and Tables 9 and 10.

Curves of sample weight loss for the flaming tests of the hydraulic fluid are shown in Fig. 33. Increasing the ambient temperature to 100°C increases the mass loss rate but has little effect on the time of ignition. At 300°C peak mass loss rates exceed 10 mg/cm^2-s (about twice the room-temperature value), and ignition occurs much earlier. At all temperatures there is no measurable char residue.

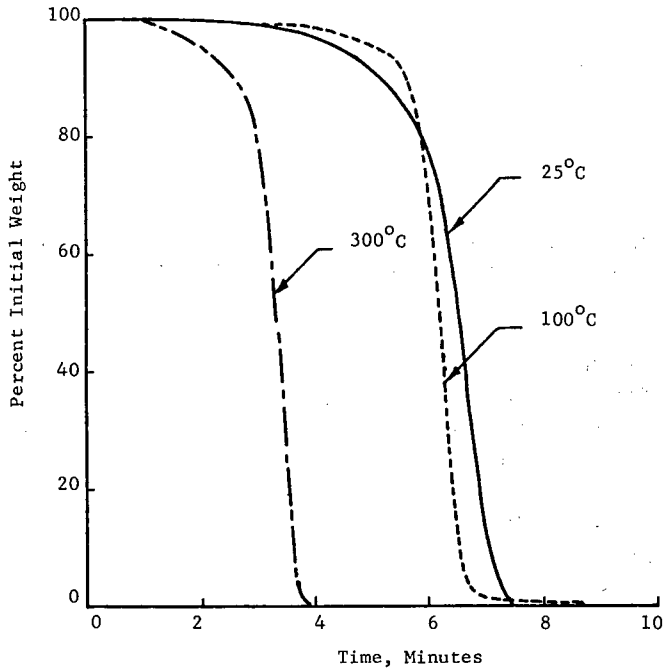

Fig. 33 — Effect of the ventilation air temperature on the sample weight loss for flaming combustion of hydraulic fluid exposed to a radiant flux of 5 W/cm^2

Mean particle diameters D_{32} determined optically are presented in Fig. 34 for flaming tests of the hydraulic fluid. After an initial transient period, D_{32} reaches a fairly steady value of 1.3 μm which is independent of the environmental temperature. The optical density also reaches its maximum value during this period of constant D_{32}. The major effect of ventilation air temperature is to shorten the period during which flaming combustion and constant mean particle size occur, which is consistent with the increased rates of mass loss.

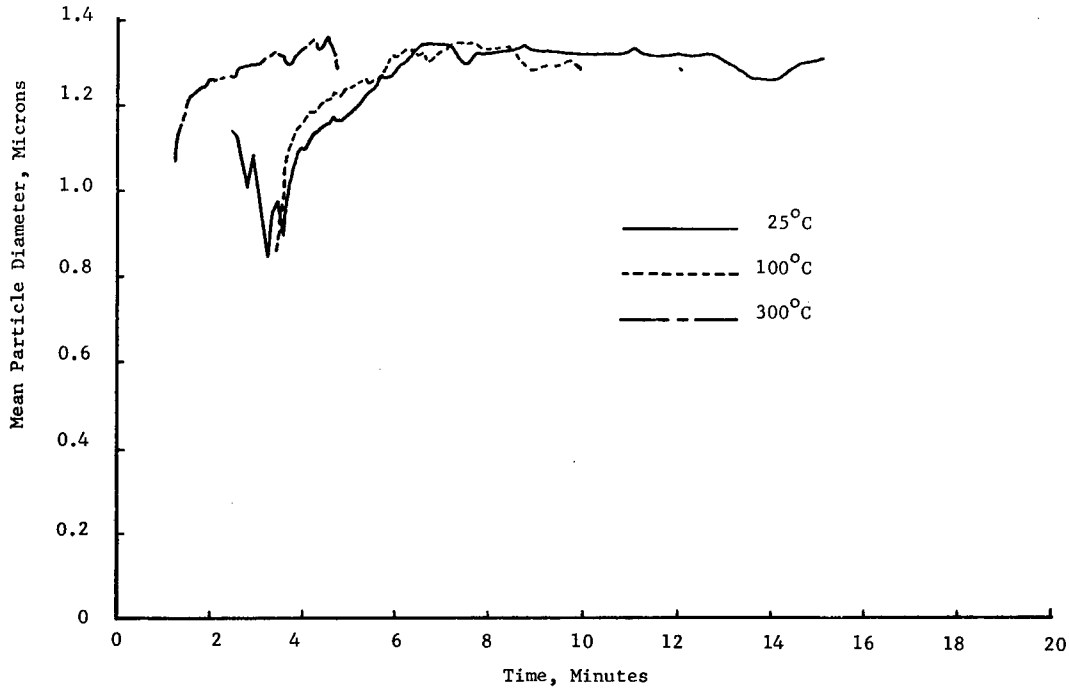

Fig. 34 — Effect of the ventilation air temperature on the smoke mean particle size for flaming combustion of hydraulic fluid exposed to a radiant flux of 5 W/cm^2

Figure 35 shows optical density variations for flaming combustion of the hydraulic fluid. The curves show that the peak optical density occurs much earlier at 300°C than at the lower temperatures due to the earlier ignition at 300°C. The corrected peak optical densities given in Table 9 show little effect on light obscuration from increasing the air temperature to 100°C and show a moderate (30%) increase in optical density from a further temperature increase to 300°C. The apparent decreases in optical density from the increases in ambient temperature shown in Fig. 35 result from the increased flow rate of the ventilation air at higher temperatures.

Smoke Particle Refractive Index and Volume Fraction

Due to the limited number of nonflaming data obtained for the hydraulic fluid, refractive index measurements are not available for the smoke particles produced by this material under nonflaming combustion. For *flaming* tests of the hydraulic fluid, the 90°-scattering ratios measured ($I_{\parallel}/I_{\perp}$) are consistent with the Mie theory for the soot refractive index $m_R = 1.57 - 0.56i$. Just as for the wall insulation material and the PVC cable jacket materials, optical density ratios (OD_R/OD_B) measured for the soot particles produced by the burning hydraulic fluid were about 20% lower than the theoretical values for spherical particles. Again it appears that the soot particles produced in flaming tests of the hydraulic fluid are nonspherical.

UNCLASSIFIED

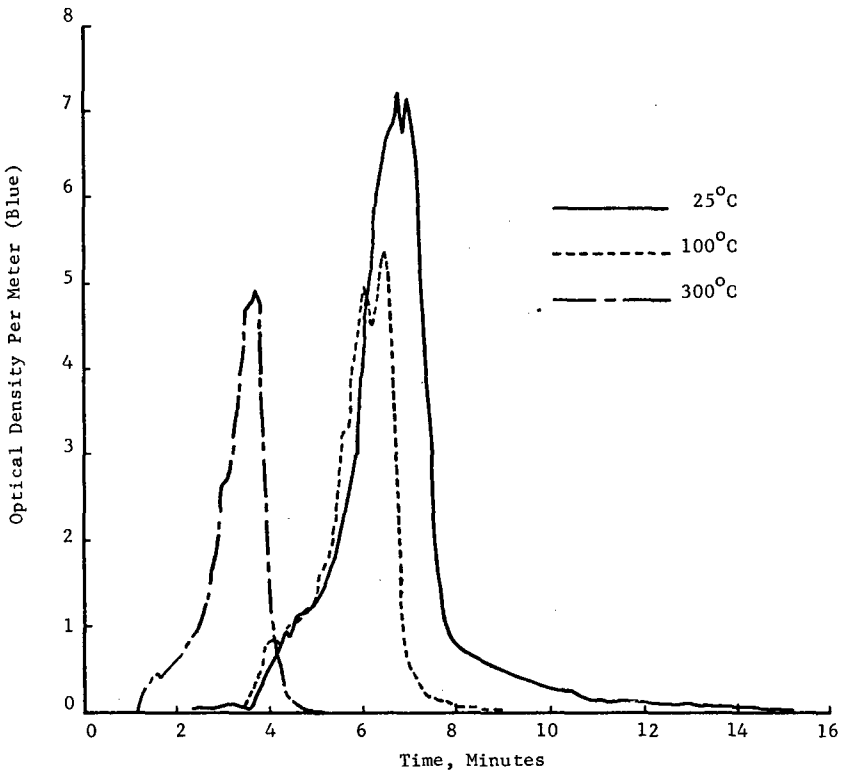

Fig. 35 — Effect of the ventilation air temperature on the smoke optical density for flaming combustion of hydraulic fluid exposed to a radiant flux of 5 W/cm^2

Table 9 — Smoke Properties Data for Hydraulic Fluid

Mode	Ventilation Air Temperature (°C)	Γ	OD_{max}		D_{32}* (μm)	Time to Peak OD (min)
			Blue	Red		
Nonflaming†	25	—	1.23	1.27	1.23	5.9
Flaming	25	0.028	7.18	5.49	1.33	6.9
Flaming	100	—	6.73	5.10	1.31	6.5
Flaming	300	—	9.41	7.02	1.31	3.7

*Averages for data points near the time of maximum optical density.
†During the initial nonflaming phase; spontaneous ignition occurred 5.9 minutes after initiation of exposure.

Volume fractions were calculated for the flaming tests of the hydraulic fluid using $m_R = 1.57 - 0.56i$. These results, which are corrected to the standard flow rate, are presented in Fig. 36 and in Table 10. These curves have shapes similar to those of the optical density curves given in Fig. 35. Raising the ventilation air temperature to 100°C has little effect on the peak volume concentration of the soot particles, and a further increase to 300°C results in a moderate increase (about 20%) in the peak volume fraction of the smoke. Also, the volume concentration peak occurs much earlier at 300°C, coinciding with the optical density peak. Increased ambient temperature has the opposite effect on the total particulate volume, however, because the total volume of smoke produced at 100°C and 300°C is about 25% less than that produced in the room-temperature atmosphere (Table 10). With the assumption of a soot particle density of 2.0 g/cm^3, the total particulate mass implied by the optically determined soot volume for the 25°C test is nearly 13 times greater than the particulate mass obtained by sampling. This discrepancy in the total particulate masses obtained by the optical and sampling techniques is further evidence that the soot particles produced by flaming combustion of the hydraulic fluid are highly non-spherical.

CHEMICAL ANALYSIS OF MAJOR TOXIC VOLATILE SPECIES IN SMOKE FROM THE WALL INSULATION MATERIAL, CABLE JACKET, AND HYDRAULIC FLUID

The toxic nature of many combustion products of polymeric materials has been well documented [11,12]. Our approach to the identification of toxic compounds in the smoke produced by combustion of the tested samples has been to chemically identify major components and then to determine their toxicity by comparison with established toxicological data [13]. However, for certain specific compounds of known high acute toxicity (such as HCl, HCN, and acrolein), their likely presence in many smoke products of combustion have led us to specifically seek to show their presence or absence in the smoke produced from the samples. For example, acrolein has a toxicity rating (LD_{50}) [13] 600 times that for acetaldehyde. Consequently it is necessary to determine its presence or absence at much lower levels than for acetaldehyde in order to determine whether it could represent a significant toxic hazard in the smoke from a particular material.

Our dual concern has been to identify toxic compounds both in the vapor phase of the smoke and also adsorbed onto the particulate components of the smoke. It has been suggested [12] that toxic substances adsorbed onto particulates can be carried to the lower lung, bypassing body defenses and so having an effective toxicity far in excess of that predicted from their concentration on the particulates.

Experimental Procedure

The pyrolysis-collection system constructed for the determination of volatile compounds is shown in Fig. 37. The major components of the system are a combustion chamber, a filter for particulate collection, a six-port valve, and a packed collection trap. All interconnecting stainless steel tubing is Teflon lined and heated to 120°C in order to avoid loss of materials by condensation on the walls. Instruments used for separation and

UNCLASSIFIED

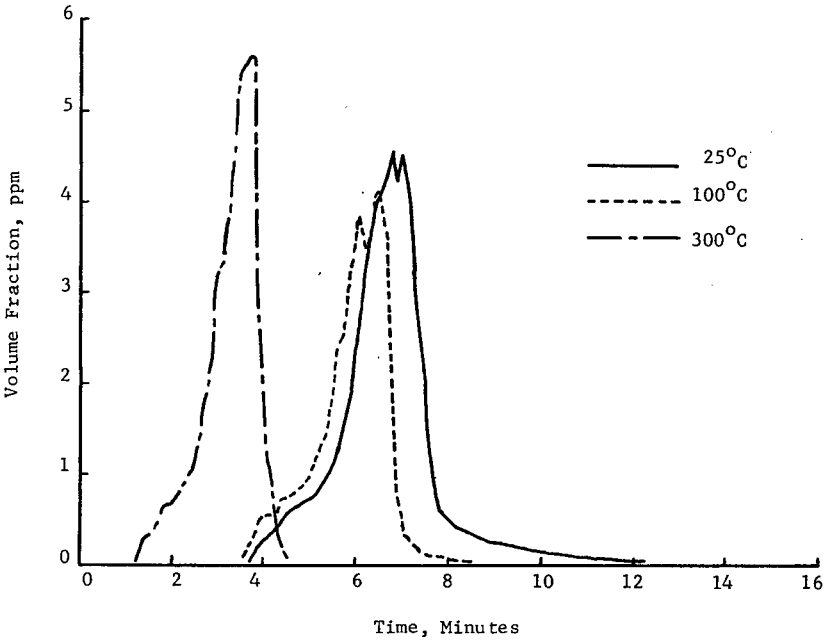

Fig. 36 — Effect of the ventilation air temperature on the particulate volume fraction for flaming combustion of hydraulic fluid exposed to a radiant flux of 5 W/cm^2

Table 10 — Sample Weight Loss and Smoke Concentration Data for Hydraulic Fluid

Mode	Ventilation Air Temperature (°C)	Peak Mass Loss Rate (mg/cm^2-s)	Peak Volume Fraction* (ppm)	Total Particulate Volume* (cm^3)	$\frac{\Gamma}{\Gamma_{25}}$
Nonflaming†	25	0.14	0.83	0.32	—
Flaming	25	5.6	4.54	3.61	1.00
Flaming	100	9.8	4.11	2.60	0.72
Flaming	300	11.1	5.58	2.68	0.74

*Based on $m_R = 1.50 - 0.0i$ for nonflaming combustion and m_R $1.57 - 0.56i$ for flaming combustion at a standard flow rate of 425 l/min.

†During the initial nonflaming phase; spontaneous ignition occurred 5.9 minutes after initiation of exposure.

identification of compounds produced during pyrolysis experiments were a Hewlett-Packard model 5710A gas chromatograph with flame ionization detector, a Hewlett-Packard model 5720A gas chromatograph with a thermal conductivity detector, and a Hewlett-Packard model 5700A/5982A gas chromatograph/mass spectrometer system with a combined electron impact/chemical ionization source and a model 2100S microprogrammable systems computer for data collection and peak identification [14].

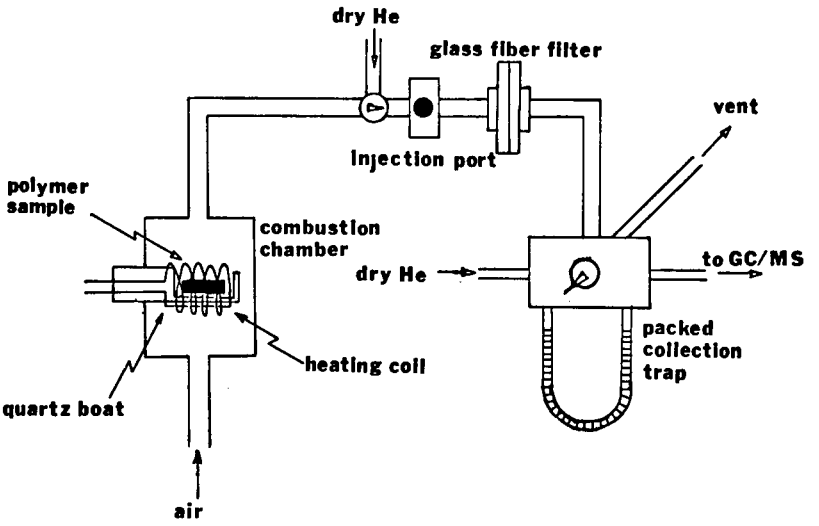

Fig. 37 — Pyrolysis-collection system for volatile compounds

The collection trap was a 20-cm by 0.635-cm-o.d. Teflon-lined stainless steel tube, packed with Porapak R (887 mg). During collection the trap was cooled with dry ice/acetone. Desorption of the collected volatiles into the gas chromatograph or gas chromatograph/mass spectrometer was produced by flash heating the trap to a predetermined temperature. Both the collection trap and the chromatographic column were packed with Porapak R (80/100 mesh), as this has been found to have superior efficiency for many of the compounds of interest in this study (such as HCN and acrolein) when compared to some of the more commonly used chromatographic materials such as Tenax-GC.

The procedure used for sequential identification of vapor phase combustion products and volatile compounds absorbed onto smoke particulates is as follows: the weighed polymer sample is oxidatively pyrolyzed in the chamber under conditions of controlled temperature and air ventilation; both vapor and smoke particulates pass through the heated, Teflon-lined stainless steel transfer lines to a Gelman glass fiber filter (type AA), which removes the particulates from the gas stream; the vapor phase is collected and concentrated on the solid adsorbent collection trap, maintained at -78°C; when combustion is complete, the system is purged with dry helium; the collection trap is heated rapidly to 150°C for 5 minutes and then temperature programmed to 200°C at 4°C per minute; following analysis of the gas phase, the particulates are heated to 50°C under a stream of

UNCLASSIFIED

dry helium, the desorbed volatiles are collected on the cooled trap, and the volatile chromatographed; and the sample boat with any ash remaining, together with the filter plus particulates, are reweighed to determine the weight loss of polymer and the yield of particulate smoke. It is necessary to dry the particulate/filter in a dessicator prior to determination of particulate yield.

Results and Discussion

The basic mass loss relationships, showing the total sample mass, ash mass, particulate mass and hence, by difference, vapor mass for the three sample types are shown in Table 11.

Table 11 — Mass Loss Data

Sample Type	Sample Mass (mg)	Ash Mass (mg)	Particulate Mass (mg)	Vapor Mass (mg)
Wall insulation material	27.34	15.71	0.41	11.22
Cable jacket	10.33	2.77	0.31	7.25
Hydraulic fluid	22.22	0.29	0.67	21.26

The chromatograms for vapor phase combustion products are shown in Figs. 38, 39, and 40. The chromatograms for the vapor phase products released from the particulates are essentially identical and are not shown here. Of course, these showed much lower concentrations of species, varying from approximately 4% of the vapor phase concentration for involatile compounds such as benzene to less than 1% for gases such as CO.

The major peaks in the chromatogram for the wall insulation material (Fig. 38) are identified in Table 12. The major toxic compounds identified were carbonyl sulfide, acetic anhydride, and benzene. Acrolein and HCN could not be detected.

The major peaks in the chromatogram for the PVC-1 cable jacket (Fig. 39) are identified in Table 13. The major toxic species identified, aside from CO, are benzene and to a lesser extent the two chlorinated species, 3 chloro 2 methyl propene and 1,4 dichlorobutane. HCl, which was determined by precipitation of AgCl from a $AgNO_3$ solution, was found to be present in large quantities in both the vapor phase and also adsorbed onto the particulates.

The chromatogram for the hydraulic-fluid combustion products is shown in Fig. 40, and the peaks are identified in Table 14. This sample produced some extremely toxic products, namely acrolein and methacrolein, in addition to benzene and CO. Acrolein and methacrolein were present in concentrations that would certainly represent a significant toxic hazard in the smoke from this sample.

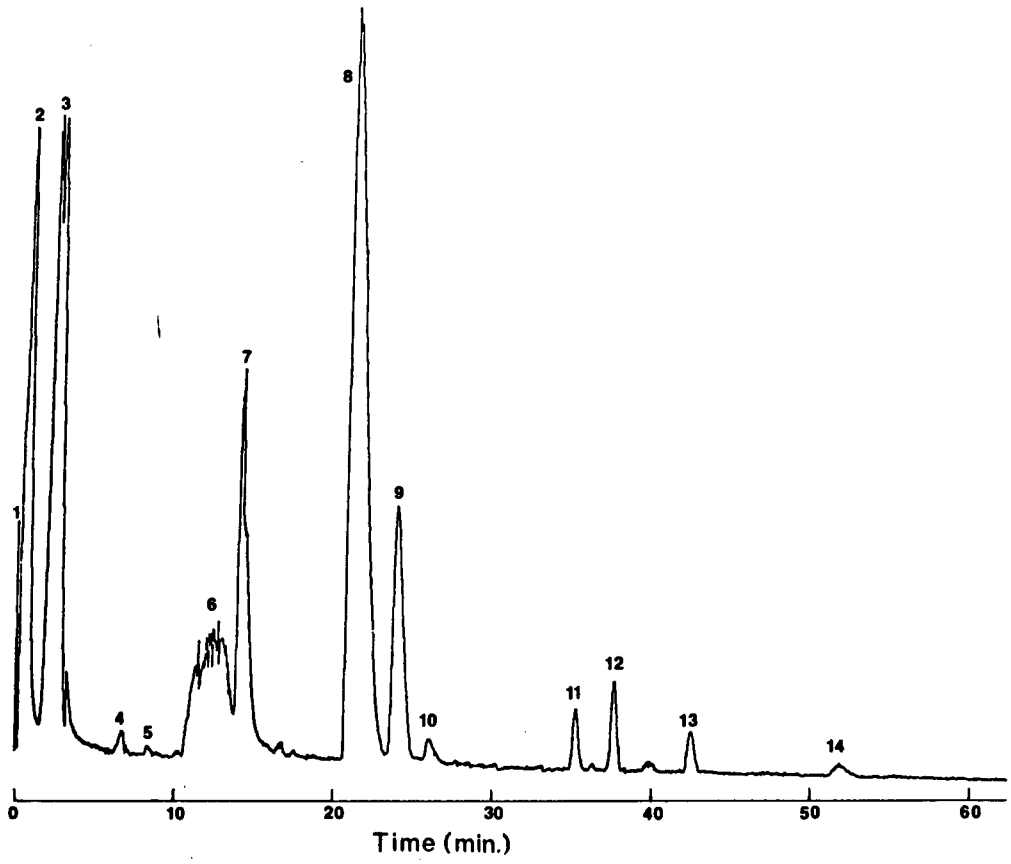

Fig. 38 — Gas-chromatograph (GC) trace for volatile compounds from wall insulation material. The peak numbers are identified in Table 12.

Table 12 — Major Volatile Components from Wall Insulation Material

Peak Number (from Fig. 38)	Compound	Concentration (mg/m^3)
1	CO	200
2	Air	—
3	CO_2	2000
4	COS	30
5	Propene	20
6	H_2O	2000
7	Acetaldehyde	100
8	Ethanol (impurity)	—
9	Acetone	200
10	Acetic anhydride	10
11	Benzene	60
12	Dioxan	70
13	Toluene	40
14	Ethyl benzene	60

*Calculated on the basis of a 10-ft by 10-ft bulkhead burning into a 25,000-ft^3 space. The data are for the vapor phase. Values for compounds adsorbed onto particulates range from 1 to 4% of the values shown.

UNCLASSIFIED

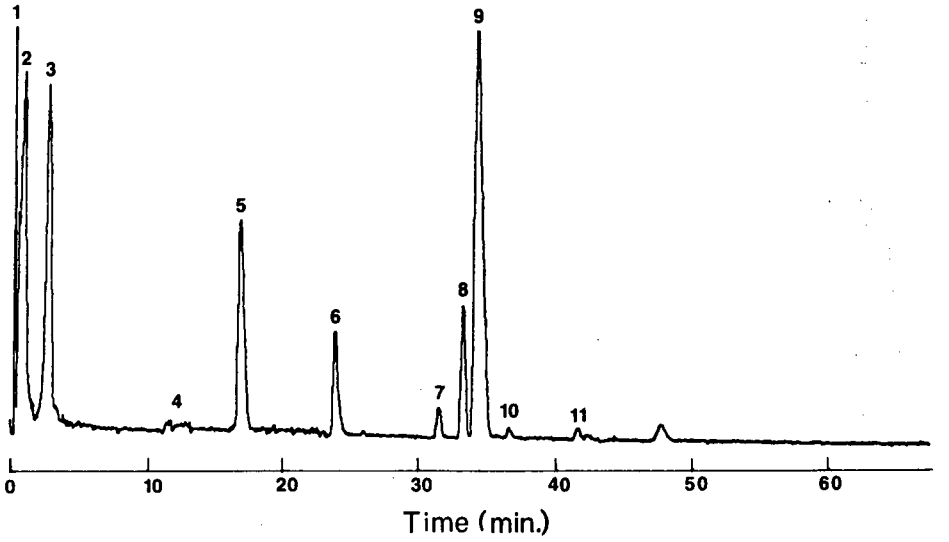

Fig. 39 — GC trace for volatile compounds from cable insulation

Table 13 — Major Volatile Components from Cable Jacket

Peak Number (from Fig. 39)	Compound	Concentration† (mg/m^3)
1	CO	3
2	Air	—
3	CO_2	53
4	H_2O	32
5	1,3 Butadiene	3
6	Acetone	3
7	3 Chloro 2 methyl propene	3
8	1,4 Dichlorobutane	1
9	Benzene	9
10	Acetic acid	1
11	Toluene	2

*HCl was identified separately, using a nonchromatographic method.
†Calculated on the basis of a 3-ft length of cable burning into a 25,000-ft^3 space. The data are for the vapor phase. Values for compounds adsorbed onto particulates range from 1 to 4% of the values shown.

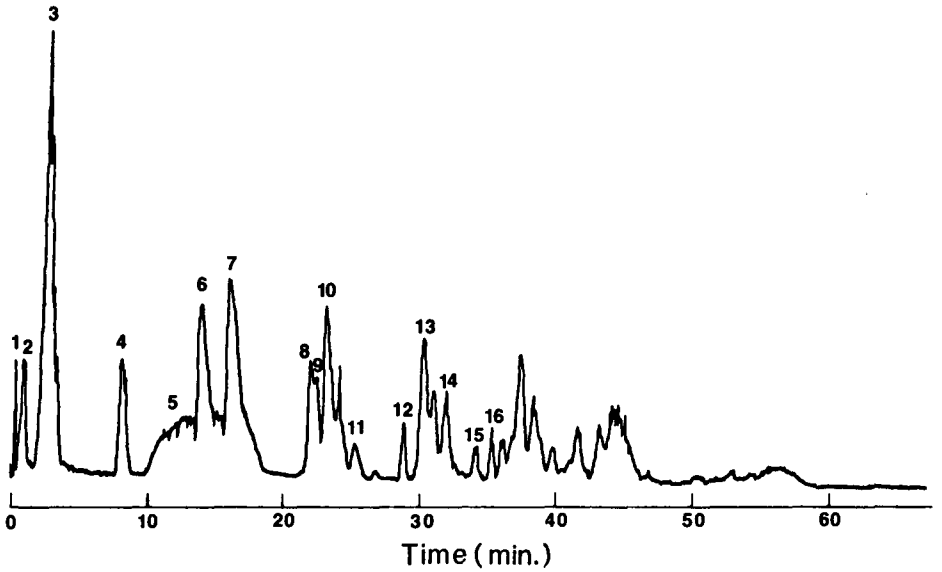

Fig. 40 — GC trace for volatile compounds from hydraulic fluid

Table 14 — Major Volatile Components from Hydraulic Fluid

Peak Number (from Fig. 40)	Compound	Concentration* (mg/m^3)
1	CO	600
2	Air	—
3	CO_2	10000
4	Propene	700
5	H_2O	7000
6	Acetaldehyde	2000
7	Butene	2000
8	Acrolein	200
9	Propionaldehyde	800
10	Acetone	2000
11	1,3 Heptadiene	400
12	Methacrolein	300
13	5-Heptan-2-one	800
14	Cycloheptane	1000
15	Benzene	800

*Calculated on the basis of a 20-gal sample burning into a 25,000-ft^3 space. The data are for the vapor phase. Values for compounds adsorbed onto particulates range from 1 to 4% of values shown.

UNCLASSIFIED

CHEMICAL ANALYSIS OF PARTICULATE SMOKE FOR POSSIBLE SMOKE PRECURSORS

To gain further background knowledge relating smoke formation processes to the chemical nature of the reaction, we have attempted to gain some useful knowledge with our three samples. Specifically these have been burned under both nonflaming and flaming conditions in the Georgia Tech combustion products test chamber. A thermal flux of 5 W/cm^2 was used in all cases, together with a ventilating air flow of 425 l/min. Ignition, when flaming combustion was used, was initiated with a propane pilot flame.

The chemical analysis data for the particulate combustion products of the wall insulation material, cable jacket (PVC-1), and hydraulic fluid are shown in Table 15. The analytical technique used was that described by Liao and Browner [15]. The major polynuclear aromatic hydrocarbon products found in the smoke of each sample are identified in Table 16.

Some interesting observations can be made from these data. With the wall insulation material, the yield of particulate smoke was very similar in both flaming and nonflaming modes of combustion. However, with smoke resulting from flaming combustion, the percentage of extractable organic compounds was much less (28% compared to 97%). Of the extractable organics in the particulate smoke, approximately the same percentage (15%) were found to be polynuclear aromatic hydrocarbons in both flaming and nonflaming combustion modes. This would indicate that the polynuclear aromatic hydrocarbons found (anthracene and pyrene) do not play the role of intermediates in the formation of the carbonaceous black smoke formed during flaming combustion. By way of confirmation of this deduction, the yields of polynuclear aromatic hydrocarbons of the other two samples were approximately in the same ratio to non-polynuclear-aromatic-hydrocarbon organic extractables as with the wall insulation material. We can therefore surmise that all the polynuclear aromatic hydrocarbons that are observed in these experiments are stable by-

Table 15 — Particulate Combustion Products of the Tested Materials

Test	Sample Mass (g)	Particulate Smoke (mg)	Extractable Organics (mg)	Polynuclear Aromatic Hydrocarbons (mg)	Aliphatic and Others (mg)
Wall insulation material:					
nonflaming	7.50	35	34	0.5	33.5
flaming	7.60	41	11.5	1.5	10
Cable jacket, flaming	16.4	128	17.5	2.5	15
Hydraulic fluid, flaming	20	145	20	2	18

Table 16 — Major Polynuclear-Aromatic-Hydrocarbon Species Found in Particulate Smoke of the Samples

Sample	Major Polynuclear Aromatic Hydrocarbon Identified	
Wall Insulation	Anthracene/phenanthrene (178)* Pyrne (202)	
Cable jacket	Anthracene (178)	0.5%
	Fluoranthene (202)	27%
	Pyrene (202)	44%
	1,2, Benzothorene or Methyl pyrene (216)	4%
	2,13 Benzothoranthene (226)	8%
	Chrysene, benzoanthracene triphenylene (228)	16%
	2,4 Benzo (a) pyrene (252)	0.3%
Hydraulic fluid	Anthracene/phenanthrene	1%
	Fluoranthene	29%
	Pyrene	45%
	1,2, Benzothorene, etc.	6%
	2,13 Benzothoranthene, etc.	12%
	2,4 Benzo (a) pyrene	0.7%

*Molecular weight.

products of whatever reactions lead to smoke formation. The evidence would indicate that they do not play a role as reactive intermediates in particulate smoke formation. Detailed understanding of the processes which do lead to particulate smoke must therefore await more complex mechanistic studies.

SUMMARY AND CONCLUSIONS

Under Task A of this program, smoke physical properties were determined for the following three classes of shipboard materials: a wall insulation material, PVC cable jacket materials, and a hydraulic fluid. These properties were determined for both smoldering and flaming combustion in both room-temperature and high-temperature atmospheres. The results of these tests are summarized below:

- For the wall insulation and PVC cable jacket, the particle size distribution is log-normal, with the smallest mass median diameters and largest geometric standard deviations obtained during flaming combustion.

UNCLASSIFIED

- Under flaming combustion, all three materials produce black smoke consisting of nonspherical soot aggregates with a mean particle diameter (D_{32}) between 1.0 and 1.3 μm and a refractive index of about $1.57 - 0.56i$.

- Under smoldering combustion, the wall insulation and PVC cable jackets produce smoke consisting of spherical tarry liquid droplets with D_{32} ranging from 0.4 to 1.5 μm. The wall insulation produces smoke particles which scatter but do not absorb light, and the smoke produced by the PVC is moderately light absorbing with a complex refractive index which varies with wavelength.

- Each of the materials converts about 2.5% of its total mass loss into smoke particulates during flaming combustion. During smoldering combustion these same materials yield 6 to 8% of their total mass loss as particulates.

- The hydraulic fluid and the PVC cable jacket materials produce strong light obscuration under flaming combustion (about 6 m^{-1}), but the wall insulation material produces much less light attenuation (about 2 m^{-1}). For smoldering combustion all three materials produce moderate light obscuration (1 to 2 m^{-1}).

- For nonflaming combustion of the wall insulation and PVC-2 cable jacket, increasing the ambient temperature decreases the mean particle diameter, the peak optical density, the peak volume fraction, and the total particulate volume. This effect is strongest for the wall insulation material, and it is consistent with a condensation mechanism for smoke production.

- For flaming combustion of the wall insulation material, increasing the ambient temperature increases the mass loss rate, resulting in more fuel-rich combustion. This slightly increases the smoke mean particle diameter D_{32} and significantly increases the peak optical density and the peak volume fraction of the smoke. This effect is weaker for the hydraulic fluid and is not observed for the PVC-2 cable jacket.

- Ambient temperature has little effect on the total volume of smoke particulates produced by these three materials during flaming combustion.

The smoke properties of these materials may also be compared with similar materials tested previously. Under nonflaming combustion the smoking tendency Γ of the wall insulation material is similar to that obtained previously for a flexible polyurethane foam [16], and under flaming conditions the wall insulation material exhibits more than twice the smoking tendency of the polyurethane foam. Also the wall insulation material produces considerably more light attenuation than the previously tested polyurethane foam under both modes of combustion. The smoking behavior of the PVC-1 cable jacket is similar to that of a previously tested PVC formulation containing a plasticizer (6-10 phthalate), a lead stabilizer, and a lubricant [4,17]. These two materials produced similar curves of D_{32} and optical density versus time, similar maximum optical densities and characteristic mean particle diameters, and similar low amounts of char residue. The smoke characteristics of the PVC-2 cable jacket, however, more closely resembles those of a previously tested PVC formulation containing the fire retardant alumina trihydrate ($Al_2O_3 \cdot 3H_2O$) in addition to the plasticizer, stabilizer, and lubricant [4,17]. Both materials leave about 25% of their

initial weight as char under low-temperature nonflaming conditions, and both exhibit similar mean particle size variations with time for both flaming and nonflaming combustion. The Navy PVC-2 cable jacket, however, produces about twice as much light attenuation under flaming combustion and half as much light attenuation under smoldering conditions as the previously tested fire-retarded PVC.

The chemical analysis work conducted under task B revealed that the three shipboard materials tested released a number of toxic substances during nonflaming combustion. All of these were detected both in the vapor phase and adsorbed onto the particulate smoke.

During smoldering combustion, all three materials released carbon monoxide and benzene, and the wall insulation material also produced carbonyl sulfide, the PVC cable jacket also produced hydrogen chloride, and the hydraulic fluid also produced acrolein and methacrolein.

Analysis of the particulate smoke products from the samples for both flaming and nonflaming combustion showed that the polycyclic aromatic hydrocarbon species determined were probably stable byproducts of the smoke formation process, rather than "frozen" derivatives of reactive intermediates.

REFERENCES

1. C.P. Bankston, R.A. Cassanova, E.A. Powell, and B.T. Zinn, "Initial Data on the Physical Properties of Smoke Produced by Burning Materials Under Different Conditions," J. Fire and Flammability 7, 165 (1976).
2. B.T. Zinn, E.A. Powell, R.A. Cassanova, and C.P. Bankston, "Investigation of Smoke Particulates Generated During the Thermal Degradation of Natural and Synthetic Materials," Fire Research 1, 23 (1977).
3. E.A. Powell, R.A. Cassanova, C.P. Bankston, and B.T. Zinn, "Combustion-Generated Smoke Diagnostics by Means of Optical Measurement Techniques," in *Experimental Diagnostics in Gas Phase Combustion Systems* (Progress in Astronautics and Aeronautics, Vol. 53), edited by Ben T. Zinn, American Institute of Aeronautics and Astronautics, New York, 1977, p. 449.
4. B.T. Zinn, R.A. Cassanova, C.P. Bankston, R.F. Browner, E.A. Powell, J.U. Rhee, and K. Kailasanath, "Investigation of the Properties of the Combustion Products Generated by Building Fires," Final Report of National Bureau of Standards grant G7-9001, Nov. 1977.
5. R.D. Cadle, *Particle Size*, Reinhold, New York, 1965.
6. R.A. Dobbins, L. Crocco, and I. Glassman, "Measurement of Mean Particle Sizes of Sprays from Diffractively Scattered Light," AIAA J. 1, 1882-1886, (1963).
7. R.A. Mugele and H.D. Evans, "Droplet Size Distribution in Sprays," Industrial Engineering Chemistry 43, 1317-1324 (June 1951).
8. R.A. Dobbins and G.S. Jizmagian, "Optical Scattering Cross-Sections for Polydispersions of Dielectric Spheres," J. Optical Society of America 56, 1345-1350 (Oct. 1966).

UNCLASSIFIED

9. M. Kerker, *The Scattering of Light and Other Electromagnetic Radiation*, Academic Press, New York and London, 1969.

10. W.H. Dalzell, G.C. Williams and H.C. Hottel, Combustion and Flame 14, 161 (1970).

11. J. Michal, "Toxicity of Pyrolysis and Combustion Products of Poly(vinyl chloride)," Fire and Materials 1, 57 (1976).

12. J.P. Stone, "Transport of Hydrogen Chloride by Water Aerosol in Simulated Fires," J. Fire & Flammability/Combustion Toxicology 2, 129 (May 1975).

13. N.I. Sax, *Dangerous Properties of Industrial Materials*, 4th edition, Van Nostrand Reinhold, New York, 1975.

14. R.O. Gardner, and R.F. Browner, "A System for the Determination of Volatile Species in the Vapor Phase and Adsorbed onto Polymer Smoke Particulates, Using Gas Chromatography and Gas Chromatography/Mass Spectrometry," Anal. Chem. (1979), submitted for publication.

15. J.C. Liao, and R.F. Browner, "Determination of Polynuclear Aromatic Hydrocarbons in Poly-(Vinyl Chloride) Smoke Particulates by HPLC and GC/MS," Anal. Chem. 50, 1683 (1978).

16 B.T. Zinn, C.P. Bankston, R.F. Browner, E.A. Powell, K.T. Joseph, J.C. Liao, M. Pasternak, and R.O. Gardner, "Investigation of the Properties of the Combustion Products Generated by Building Fires," Final Report of the Products Research Committee Project, Jan. 1979.

17. B.T. Zinn, C.P. Bankston, R.F. Browner, E.A. Powell, K.T. Joseph, M. Pasternak, R.O. Gardner, K. Kailasanath, "Investigation of the Properties of the Combustion Products Generated by Building Fires," Final Report of National Bureau of Standards grant G8-9003, Nov. 1978.